Flow, Turbulence and Combustion (2024)

On the feasibility of a self-adaptive strategy for hybrid RANS/LES based on physical criteria and its initial testing on low Reynolds number backward-facing step flow

Martin David · Mahitosh Mehta · Rémi Manceau

Received: 22 May 2024 / Accepted: 6 September 2024

Abstract Hybrid RANS/LES methods can produce more reliable results than RANS with a reasonable computational cost. Thus, they have the potential to become the next workhorse in the industry. However, in continuous approaches, whether or not they depend on the grid step explicitly, the ability of the model to switch to a well-resolved LES depends on the mesh generated by the user, such that the results are user-dependent. The present paper proposes a self-adaptive strategy, in which the RANS and LES zones are determined using physical criteria, in order to mitigate the user influence. Starting from an initial RANS computation, successive HTLES are carried out and the mesh is refined according to the criteria. To demonstrate the feasibility of this strategy, the method is applied to the backward-facing step case with the Hybrid Temporal Large Eddy Simulation (HTLES) approach, but is suitable for any other hybrid approach. The results obtained show that the method reaches a fixed point after only a few simulations and significantly improves the predictions when compared to RANS, with no intervention from the user. Even though the process is still a long way from being applicable to a wide range of turbulent flows, this paper is a demonstrator of the applicability of this self-adaptive strategy.

Keywords Hybrid RANS/LES, Self-adaptive strategy, Physical criteria, Active forcing, Demonstrator

1 Introduction

The Reynolds-Averaged Navier-Stokes (RANS) method makes it possible to investigate industrial cases due to its low computational cost, but often lacks reliability and only produces statistical results. The multi-physics flows encountered in combustion chambers or in solar receivers of concentrated solar power systems exhibit strong coupling between the dynamics and the heat transfer, the flows around wind turbine blades, under unsteady and turbulent atmospheric conditions, and the flows around complex geometries, such as inside the engine bay are examples for which RANS can be unreliable, leading to a poor flow estimate. The limitation of RANS models in producing satisfactory drag predictions for the flow around bluff bodies, such as flow around wind turbine mast or around the car mirrors, is notorious. Large adverse pressure gradients and separation encountered in a wide range of practical problems, such as transonic airfoils and wings, supersonic engine intakes, diffusers of centrifugal compressors, and turbo-machinery cascades are also known to be very challenging for RANS. In addition, in high-lift flows on transport aircraft, characterized by significant geometric complexity of the high-lift system, the generated high lift is associated with high suction peaks followed by strong adverse pressure gradients that may lead to separation. The accuracy of RANS methods for predicting the maximum lift coefficient and the associated incidence is generally insufficient. The reader is referred to Bush et al. [6] for a detailed review of RANS limitations. In most industrial cases, there is also a need of unsteady information to compute the fluid-structure interactions, which is lacking in RANS. This is illustrated for instance in the field of marine energy where precise unsteady

Laboratory of Mathematics and Applied Mathematics (LMAP), University of Pau & Pays Adour, E2S UPPA, CNRS, INRIA, CAGIRE project-team, 64000, Pau, France

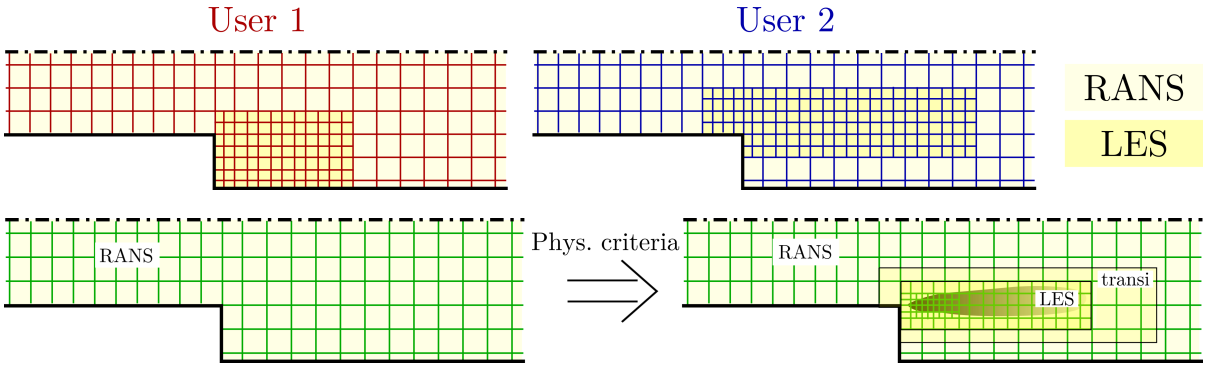

Fig. 1: Schematic view of the problem (here non-conformal grid are represented for the sake of clarity). Top: Usual user-dependent hybrid RANS/LES. Bottom: Proposed self-adaptive strategy.

information is needed to compute the loads applied on the structures. On the other hand, LES, by only modeling the small turbulence scales, generally provides more accurate results and gives access to unsteady information. However, its computational cost remains too high in wall-bounded high Reynolds number industrial configurations. Even if the computing power is expected to continue increasing, Large Eddy Simulation (LES) should remain too expensive in many domains in a foreseeable future [40].

In most cases, it is desirable to resolve a larger range of the turbulence spectrum to get more information on the flow and handle strongly swirling flows, large-scale separation, acoustics sources, *etc.* Hybrid RANS/LES models are thus very promising since they can drastically reduce the computational cost of LES, give access to time-dependent information, and provide more reliable results than RANS. In these approaches, modeled motions, associated with the RANS and the LES models, and resolved motions, associated with the unsteady modes captured in the LES region, coexist. Hybrid RANS/LES methods may be divided into two categories: zonal, or discontinuous, and non-zonal, or continuous, approaches. In the first case, two different models are used in two subdomains. The main challenge with these approaches is to deal with the boundary conditions at the interface between the two modes. In non-zonal, or continuous approaches, only one set of equations is used and the transition from RANS to LES relies on model parameters updated during the computation. Some of the most usual non-zonal hybrid RANS/LES approaches are the family of Detached Eddy Simulation (DES) models [43], the Partially-Integrated Transport Model (PITM) [8], the Partially-Averaged Navier-Stokes (PANS) method [20], and the Scale-Adaptive Simulation (SAS) [36]. The reader is referred to Chaouat [9] or [22] for recent reviews of hybrid RANS/LES methods. In many methods, the RANS-LES switching is based on the grid size. In other methods [35, 38, 21], the switching is based on criteria independent of the grid step. However, in all cases, the size of the smallest resolved vortices is inevitably linked to the grid step. The mesh designed by the user therefore has a major influence on the model's ability to switch to LES mode locally.

Most industrial flows involve complex geometry and multi-physics phenomena inducing complicated mesh generation and strong couplings. The flow through solar receiver including vortex generators for heat transfer improvement is a example of flow situations critical for industry. The future of CFD solver will probably be oriented towards the user-independence and the use of multi-fidelity approaches such as hybrid RANS/LES, which highlights the need for self-adaptive approaches for hybrid RANS/LES.

A grid convergence can always be reached in RANS computations making them theoretically user-independent. It is true that in industrial applications, the question of mesh convergence remains problematic, as it requires a great deal of time and computing resources. However, this convergence can be sought, and many efforts are being made to make this process automatic (e.g. [3]). For pure LES and hybrid RANS/LES, the situation is more complex. On the one hand, there is no longer any grid convergence of the time-dependent solution, except at the DNS limit, and it is only convergence of the flow statistics that can be sought. On the other hand, for continuous hybrid RANS/LES approaches, the model is designed to remain in RANS mode in areas where the mesh is not fine enough to achieve good LES, and so the extent of the RANS and LES zones is mesh-dependent. Guided by intuition and/or experience of the flow under consideration, along with an understanding of the limitations of RANS models, users decide to refine

the mesh in areas deemed necessary for transitioning to LES mode. This is illustrated by Fig. 1 for the example of a backstep flow: two users may generate very different meshes, yielding different LES regions and, consequently, different results. Such user influence is highly dangerous in an industrial context, and in order to ensure the reliability of CFD for the design, dimensioning, and certification of industrial systems [37, 44], mitigating the user influence is of major importance. In contrast, RANS calculations are in principle user-independent: for a given model and given boundary conditions, the grid-converged solution is unique. In hybrid RANS/LES, in particular the choice of the zone where the mesh is refined in order to switch to LES, can lead to very different results for two users. The aim of this article is to investigate the feasibility of a new methodology for making hybrid RANS/LES as user-independent as RANS.

Some approaches, often referred to as *self-adaptive*, break the explicit link between model and local grid step. The switch from RANS to LES is then driven by a physical criterion evaluated during the computation, such as the ratio between the integral and von Kármán length scales [36, 27] or the ratio of modeled to total turbulent energy [20, 38, 39, 5]. This type of models, called *second generation Unsteady RANS (URANS)* models by Fröhlich et al. [17], introduces a partial decoupling between the model and the mesh, enabling the model, for example, to decide to remain in RANS mode even if the mesh is fine. The physical criteria used enable the model to detect whether turbulent structures appear locally in the resolved field, and to reduce the turbulent viscosity or the Reynolds stresses accordingly. However, it is clear that the decoupling is not complete, since the size of the resolved structures is still constrained by the grid, and the model cannot switch to LES mode if the mesh is too coarse, such that the user's influence remains very significant.

A way of avoiding the latter problem is that the mesh size is not set by the user, but by an adaptive meshing process. A few studies have explored hybrid RANS/LES methods focused on investigating mesh self-adaptivity within a predetermined and fixed LES region. Limare et al. [29], using DES, proposed remeshing based on physical criteria, to adapt the mesh in the LES zone using a simulation strategy combining an octree-Adaptive Mesh Refinement (AMR) and overset grids. The grid size is partly controlled by one of the three following criteria, depending on the case study: the laminar-to-turbulent viscosity ratio, the von Kármán length scale-to-grid step ratio, or the Taylor length scale-to-grid step ratio. Assessing local LES-resolution sensors for hybrid RANS/LES simulations, Reuß et al. [41] performed Improved Delayed Detached-Eddy Simulation (IDDES) of a flow over a backward-facing step. They studied different formulations of a mesh sensor that detect under-resolved regions in LES region and can be used as input for automatic and local mesh refinement. Specifically, they proposed to refine the mesh in the LES region if the resolved turbulent kinetic energy is less than an arbitrary target of 80% of the total turbulent kinetic energy outside of the RANS region.

One step further is the work of Woodruff [47], in which the extent of the LES region is also self-adaptive. The location and size of the LES region are imposed by the user at the beginning of the workflow, then the region is allowed to grow until the solution becomes insensitive to this growth, and the grid size is adapted based on the local value of the strain rate. In this approach, the position of the LES zone is still determined by the user, based on a priori knowledge of the flow, but the size of this zone and the mesh refinement are determined adaptively.

In hybrid RANS/LES, the gray area mitigation is a major concern since the method suffers from excessively slow generation of resolved structures. When transitioning to LES, the model is designed to reduce the modeled energy, but there is no mechanism to transfer the equivalent amount of energy into the resolved motion, resulting in an underestimation of the total turbulent energy. There are several types of methods to generate resolved structures. Synthetic turbulence approaches are mostly based on Fourier reconstruction techniques, refer to [24] for instance. Another type of forcing aims to generate virtual vortices, either by superimposing them to the velocity field or by adding a restoring force in the momentum equation. Volume forcing methods are linked to the relative orientations of the flow and the wall and are thus weakly flexible [33]. A review of the existing methods has been performed by Keating et al. [26]. In the present study, the *active* forcing proposed by Mehta et al. is used [33], allowing to generate resolved structure with no prior information on the flow, and thus improving the flexibility of use of hybrid RANS/LES methods.

The aim of the present study is to develop a fully self-adaptive approach in which the user does not influence the definition of the RANS and LES regions and the resolution in the LES region. Starting from a RANS computation with a mesh obtained after a grid convergence study, the proposed method autonomously determines both the LES and RANS/LES transition regions, along with the size of the cells in the LES region based on physical criteria, as illustrated in Fig. 1. As RANS results are grid converged,

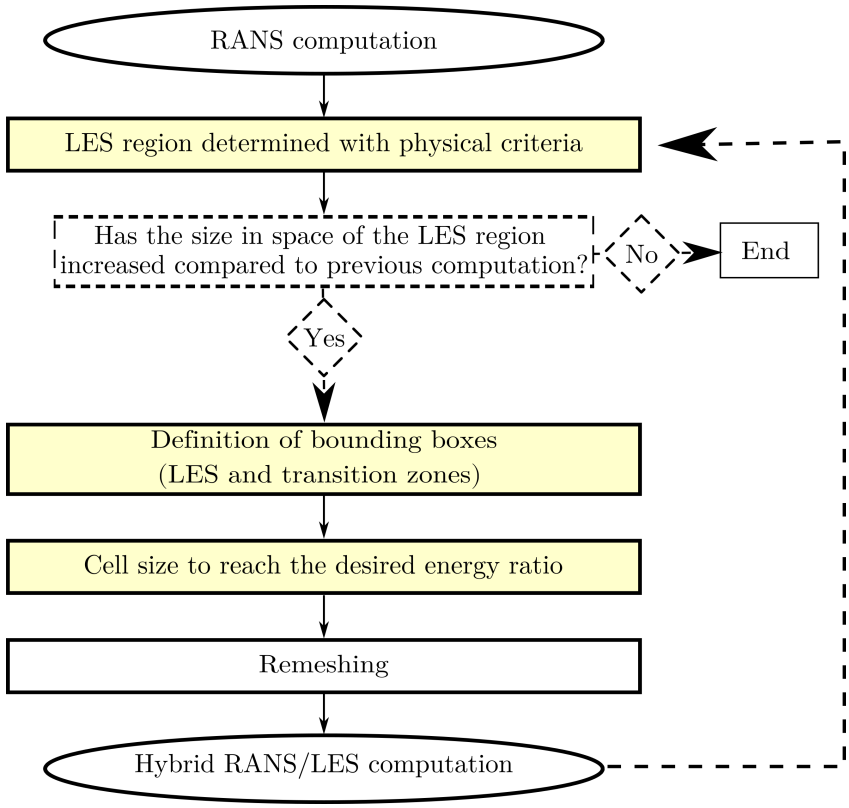

Fig. 2: Algorithm used for the self-adaptive approach.

they are considered here to be independent of the user. However, it is possible to rely on a RANS calculation with automatic mesh refinement, so as to completely avoid any user influence on the initial state of our algorithm. Successive hybrid RANS/LES computations are conducted and the characteristics of the LES and transition regions are updated after each simulation until a fixed point is reached. Here, the expression *fixed point* is used in the same sense as for sequences, i.e., the solution is identical (within a convergence tolerance) to the solution obtained at the previous iteration of the algorithm. As a demonstrator, the strategy is applied to the backward-facing step case [28] using the HTLES approach [14], in its active version [33]. Note that the purpose of this article is not to evaluate the HTLES model, which was already validated in several cases [30, 2, 13, 32] and is available is the commercial code STAR-CCM+ under the name SRH [23, 31].

The paper is organized as follows: the flow configuration is presented in section 2, our self-adaptive strategy is described in section 3, focusing on the possible physical criteria to identify the region where LES is necessary (section 3.1), the way to determine the size of the RANS/LES transition region (section 3.2), and criteria used to fix the targeted grid step in the LES region (section 3.3). The hybrid RANS/LES model used for testing this strategy, the active HTLES of Mehta et al.[33] is described in section 4. Finally, in section 5, the self-adaptive strategy is evaluated in the case of a backward-facing step, by investigating the evolution of the RANS and LES zones and the associated mesh during successive iterations of the algorithm, as well as comparing of the results with Direct Numerical Simulation (DNS) data.

2 Configuration

The demonstrator of the self-adaptive strategy is applied on the backward facing-step case, reproducing the geometry and the physical setup of the DNS of Lamballais [28], with a bulk Reynolds number $Re = U_H H/\nu = 5000$, where H is the half-width of the channel and U_H the bulk velocity downstream of the

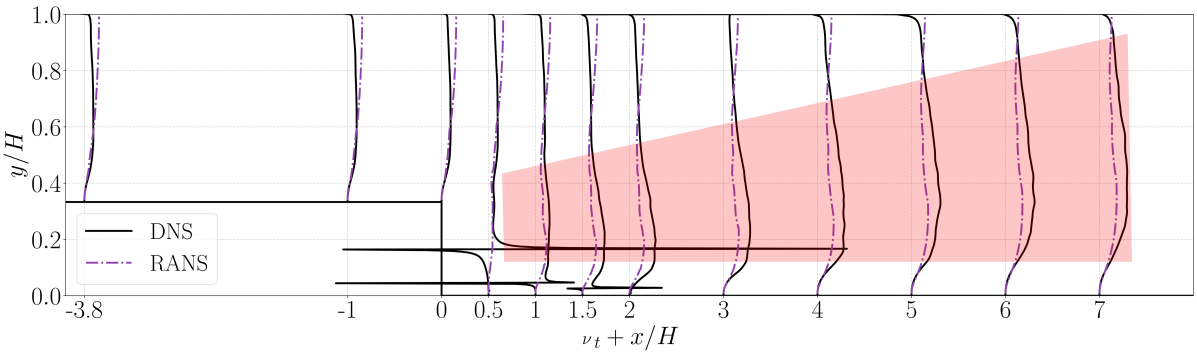

Fig. 3: Turbulent viscosity profiles in the y-direction for 12 streamwise locations. DNS results are from Lamballais [28]. The region of the main discrepancies between the RANS and DNS profiles is highlighted by the red trapeze.

expansion. The expansion ratio h/H is 2/3. Only the lower half of the domain is considered with a symmetry applied at $y/H = 1$. The extent of the computational domain is $4H$ upstream and $16H$ downstream. In the spanwise direction, the domain size is H and the flow is periodic. In the hybrid RANS/LES literature [42, 11], the spanwise extent is generally set to $2H$ to avoid any domain size effect. In the present case, we chose an extent of H to reduce computational costs. This might have a minor impact on the results, but it does not affect the main conclusions drawn about the proposed methodology. A periodic RANS channel flow computation is used as the inlet boundary condition. The RANS model is the k-ω-SST model [34].

Note that in the present work, all the computations are carried out using code_saturne, a general CFD solver developed by EDF [4], based on a finite-volume method and a fully collocated arrangement for all the variables. A standard predictor-corrector scheme (SIMPLEC) is used to solve the velocity-pressure system. The Crank-Nicholson time scheme and a second-order (upwind in the RANS zone, centered in the LES zone) convection scheme are used. For hybrid RANS/LES, the statistical quantities are evaluated using both temporal averaging and spatial averaging in the periodic direction (z).

3 Self-adaptive strategy for hybrid RANS/LES

The proposed self-adaptive strategy is summarized in Fig. 2. This method aims at autonomously determining the LES and transition zones as well as the cell size in the LES zone. It consists in successive simulations to iteratively update the zones and the cell size until the LES region remains stable. More precisely, the algorithm is initialized by a grid-converged RANS calculation. The RANS results are used to evaluate, based on a physical criterion, in which region to switch to LES mode. Two nested boxes are defined, delimiting the LES region and the RANS/LES transition region. The mesh in these two boxes is then refined to satisfy a resolution criterion. A new calculation is performed in hybrid RANS/LES using this automatically refined mesh. The physical criterion for determining the LES zone is updated on the basis of the average solution obtained in this hybrid RANS/LES simulation. Practically, after each computation, the statistically averaged quantities are used to determine the LES region and the local grid requirements for LES for the next one. These instructions are provided to the remeshing tool (GMSH [19]) to generate the grid for the next computation. If the LES zone is larger than previously, then a new iteration of the algorithm is performed. Currently, each new computation is started from scratch with adapted zones and mesh. With view to disseminate the methodology in industry, it would be beneficial to project the velocity and pressure fields on the new mesh to restart the computation. This would decrease the computational cost and make the strategy more cost-effective. Otherwise, the algorithm stops and the solution obtained at this iteration is the result of the auto-adaptive process. This result is not necessarily the closest possible to DNS: an expert user could potentially achieve a better adaptation of the LES zone and the mesh could be further refined, but it is worth recalling that the aim is precisely to have a method that does not depend on the user's expertise. Furthermore, in an industrial context, the aim is not to achieve a very fine LES, but to improve RANS results by switching to LES in the appropriate zones.

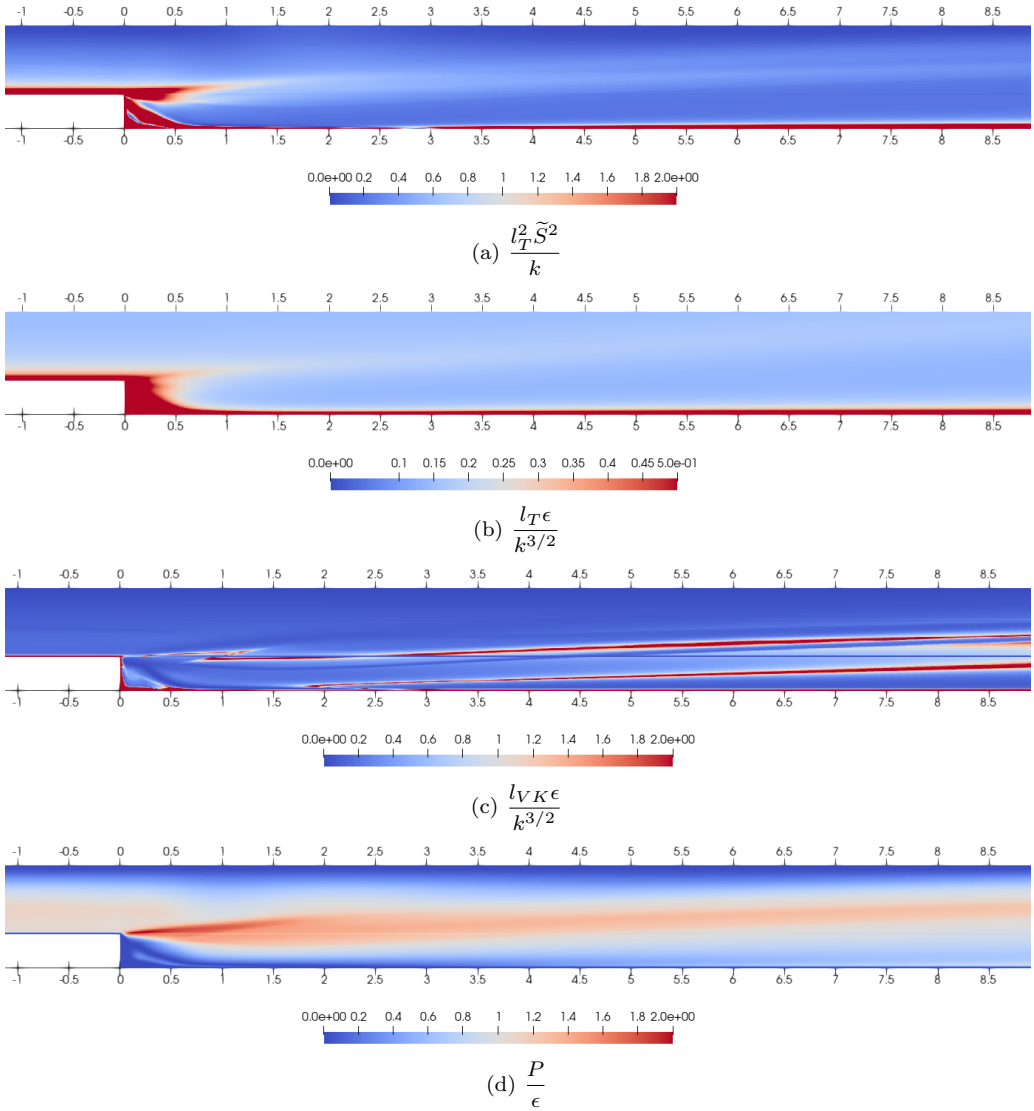

Fig. 4: Isocontours of some candidate physical criteria for defining the interface between RANS and LES.

The three steps highlighted in yellow correspond to pivotal aspects of the present study and are detailed in subsections 3.1, 3.2, and 3.3.

3.1 Where to switch to LES?

It is desirable to switch to LES in regions where the RANS computation may not be reliable, and to identify this region by applying criteria that can be evaluated from the RANS results only, without recourse to comparison with experimental or DNS data, which are not generally available in an industrial configuration. In order to identify a relevant criterion, in this section, we compare in Fig. 3 the RANS turbulent viscosity against the equivalent DNS turbulent viscosity $\nu_t \approx -\langle u'v' \rangle / (\partial U / \partial y)$ computed from the data from Lamballais [28]. The equivalent DNS turbulent viscosity exhibits singularities where the velocity gradient is zero. Apart from these singularities, the region where the largest discrepancies are observed between RANS and DNS is highlighted by the red trapeze. The aim of the remainder of this section is to

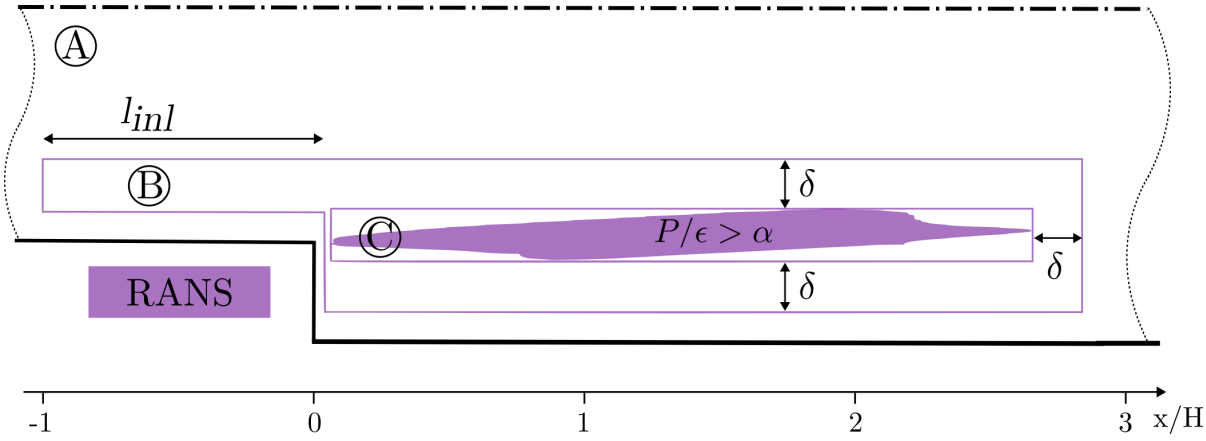

Fig. 5: Visualization of the region where $P/\epsilon > \alpha$ based the RANS computation performed with the $k-\omega$ SST model. The two bounding boxes delimit zones A, B, and C corresponding to the RANS, RANS/LES transition, and LES zones, respectively.

determine a criterion, based solely on RANS results, without using DNS data, that can be used to identify this region, in which the hybrid model must switch to LES in order to improve the results.

The physical criteria used to define the refinement region in the framework of self-adaptive hybrid RANS/LES must be

(i) based on Reynolds-averaged quantities,
(ii) independent of the grid step,
(iii) non-dimensional,
(iv) objective (independent of the reference frame).

Numerous physical criteria corresponding to the constraints listed above have been considered and evaluated on the basis of RANS results. Those that seem most relevant, at least for the case of the backward-facing step, are presented in Fig. 4. They involve the turbulent kinetic energy, k, the production of turbulent kinetic energy, P, the dissipation, ϵ, the strain rate $\widetilde{S} = \sqrt{2S_{ij}S_{ij}}$, the Taylor length scale, $l_T = \sqrt{10\nu_t k/\epsilon}$, the Von Kármán length scale, $l_{VK} = K\widetilde{S}/|H|$, where $K = 0.41$ and $|H|$ is the Frœbenius norm of the Hessian matrix of the velocity, computed as follows:

$$\|\mathbf{H}\|_F = \sqrt{\sum_{i,j}\left(\frac{\partial^2 u}{\partial x_i \partial x_j}\right)^2 + \sum_{i,j}\left(\frac{\partial^2 v}{\partial x_i \partial x_j}\right)^2 + \sum_{i,j}\left(\frac{\partial^2 w}{\partial x_i \partial x_j}\right)^2}. \quad (1)$$

Overall, the criteria studied show a sharp increase downstream of the step, then the region colored in red extends downstream and moves away from the bottom wall. This is explained by the flow separation and the development of a reattached boundary layer. In Figs. 4a and 4b, the criteria exhibit high values in the detached shear layer, the near wall region, and the beginning of the recirculation zone. As the near-wall region is intended to stay in RANS mode, they are not adopted for this self-adaptive strategy. The third criterion presented (Fig. 4c) shows three thin red zones: the first follows the wall and is mainly due to the term $\epsilon/k^{3/2}$. The second and the third zones are induced by the first-order derivative-to-second-order derivative ratio involved in the Von Kármán length scale. This criterion, which is used in SAS to identify regions where turbulent structures appear in the resolved field, is therefore unsuitable for identifying detached shear layers from a Reynolds-averaged solution. The last criterion identifies the detached shear layer satisfactorily and corresponds relatively well with the zone identified in Fig. 3, where the RANS might not be sufficient. For these reasons, it could be used in the case of the backward-facing step. Combining different criteria, able to capture numerous flow features, to make the adaptive approach ready for a wide range of applications is beyond the scope of the present paper.

Therefore, in order to demonstrate the applicability of the adaptive strategy, the criterion chosen herein is simply the production-to-dissipation ratio. This criterion makes it possible to separate the zones close

to spectral equilibrium (P/ϵ close to unity), where RANS models are generally sufficiently accurate, and the out-of-equilibrium zones where it is preferable to switch to LES mode to improve the quality of the results. Indeed, RANS models are designed and calibrated to correctly reproduce attached boundary layers, which are zones where turbulence is close to equilibrium, and are based on assumptions that are not true in out-of-equilibrium regions, such as using dissipation to calculate the integral scale and the turbulent viscosity. In the future, different criteria must be combined to cover a wide range of flows, but for the particular case of the backward-facing step, this single criterion is sufficient to demonstrate the feasibility of an auto-adaptive algorithm. Thus, regions where to switch to LES are identified via the threshold

$$\frac{P}{\epsilon} > \alpha, \tag{2}$$

where P and ϵ are the total production and total dissipation, respectively, and the threshold is chosen as $\alpha = 1.4$. Note that the case of laminar regions where P and ϵ are both zero can be treated by deactivating the switch in such regions. The computation of the production-to-dissipation ratio, which relies on quantities averaged in time and span direction, is updated at the end of each computation to adjust the LES zones from one computation to the other. Note that the value $\alpha = 1.4$ has been determined based on the results shown in Fig. 3 to achieve a relevant size for the LES region for this test case. However, for the application of the self-adaptive strategy to industrial cases, the threshold selection need to be standardized by domain experts to ensure consistency across different engineers. This criterion is not sufficient to generalize our approach, for several reasons: on the one hand, different flows with $P/\epsilon > 1$, such as homogeneous shear flows, reach a weak-equilibrium state with constant Reynolds stress anisotropies and self-similar mean velocity profiles, and are well reproduced by RANS models; on the other hand, there are many physical mechanisms difficult to reproduce in RANS [18], which requires a multi-criteria approach. However, the threshold $\alpha = 1.4$ is well suited for the backward facing step case, leading to a relevant LES zone, in relatively good agreement with the main modeling error region, as seen in Figs. 3 and 4d, such that it is used here to demonstrate with a simple criterion the feasibility of our approach. Figure 5 shows the region identified by this criterion. The total production is obtained from

$$P = -\left(\overline{u_i' u_j'} + \tau_{ij}^{\mathrm{m}}\right) S_{ij}. \tag{3}$$

$\overline{u_i' u_j'}$ is the Reynolds-averaged (in practice, averaged in time and in span), which is zero in a RANS computation. τ_{ij}^{m} is the Reynolds-averaged sub-filter stress tensor, equal to the Reynolds-stress tensor in RANS mode, and S_{ij} is the mean strain rate tensor. The total dissipation is computed as

$$\epsilon = \epsilon_{\mathrm{m}} / r_\epsilon, \tag{4}$$

where ϵ_{m} is the Reynolds-averaged sub-filter dissipation. r_ϵ is the ratio of the modeled dissipation ϵ_{m} to the total dissipation ϵ. This ratio is equal to one in RANS, and generally considered very close to one in LES mode, since the small scales are not resolved [14]. However, in low Reynolds number regions, such as the recirculation region downstream of the backstep, a small part of the dissipation can be resolved. This must be accounted for in order not to bias the evaluation of the criterion (2). The determination of r_ϵ in the framework of the HTLES model used herein is presented in section 4. Note that, to address inherently unsteady flows, the Reynolds averaging used to compute the criteria can be replaced with filtering over a short period of time that is adapted to the flow characteristics. Some work on selecting an appropriate filtering time for unsteady flows has already been conducted in the PhD thesis of Afailal [1].

3.2 How to ensure the RANS/LES transition?

Bounding boxes are defined around the region satisfying the physical criterion given by Eq. (2) in order to adapt the mesh, as shown in Fig. 5. For practical reasons, the RANS, RANS/LES transition, and LES zones are denoted A, B, and C, respectively. They are obtained using the following rules:

(i) The LES zone (zone C) is the smallest rectangle containing the $P/\epsilon > \alpha$ region.

(ii) The transition zone (zone B) is used to smoothly link the meshes used in LES and RANS zones. It is characterized by a rectangular shape bounding the LES zone with a thickness $\delta = 0.5\,\langle l_I \rangle_{P/\epsilon>\alpha}$ where $\langle l_I \rangle_{P/\epsilon>\alpha}$ is the mean of the integral length scale in the zone satisfying Eq. (2). If at the end of a simulation the region corresponding to $P/\epsilon > \alpha$ extends until the bounds of the transition zone, the thickness δ of this zone is multiplied by 10 in this direction for the next iteration of the algorithm, to reduce the total number of iterations to reach the stabilization of the adaptive method. Upstream, the beginning of the transition zone is fixed with a length of

$$l_{inl} = C_{inl}\delta, \tag{5}$$

where $C_{inl} = 5$ is a constant, which is determined by a preliminary study presented in Sec. 5.1. This is the minimal length required for the volume forcing presented in Sec. 4.2 for generating turbulent structures. Note that, since a shielding function is applied in the hybrid RANS/LES model from the wall to $y^+ = 20$ to enforce the RANS mode in the near wall region, this shielded region is excluded from zone B. The implementation of a shielding function, as described in Sec. 4 is essential to ensure the integrity of results, particularly in cases where near-wall meshes are ambiguous (fine enough to resolve turbulent structures but too coarse for wall-resolved LES). The parameters of the shielding function are not intended to be modified by the user.

(iii) The RANS zone (zone A) is the rest of the domain. The RANS mode of the hybrid RANS/LES model is imposed. In this zone, the mesh will not be refined.

3.3 What is the targeted cell size in each region?

In order to provide a user-independent method, the mesh size in the LES region must now be set by an objective criterion. The criterion chosen here is the ratio r_K of modeled energy k_m to total turbulent energy k_r. Assuming a Kolmogorov spectrum, we have

$$r_K = \frac{k_\mathrm{m}}{k} = \frac{1}{k}\int_{\kappa_c}^{\infty} E(\kappa)\mathrm{d}\kappa = \frac{3C_\kappa}{2}\left(\kappa_c \frac{k^{3/2}}{\epsilon_m}\right)^{-2/3}, \tag{6}$$

with $\kappa_c = \pi/\Delta$ the cutoff wavenumber, ϵ_m the modeled dissipation, which definition depends on the model used, and $k = k_m + k_r$. The closer r_K is to 0 the more resolved energy and the less modeled energy. Equation (6) reflects the fact that the unresolved energy scales with $\Delta^{2/3}$, and, consequently, the subgrid viscosity scales with $\Delta^{4/3}$ (see [15] for a detailed analysis). The cell size to reach the targeted energy ratio r_K is thus computed as

$$\Delta = \pi\left(\frac{2}{3}\frac{r_K}{C_K}\right)^{3/2}\frac{k^{3/2}}{\epsilon_m}. \tag{7}$$

Since it is linked to the integral length scale $k^{3/2}/\epsilon_m$, Δ is variable in space and is given as a local target to the meshing tool. The computation of the targeted cell size, which relies on quantities averaged in time and span direction, is updated at the end of each computation to adjust the cell size from one computation to the other.

The rules followed to build the new mesh are:

(i) In the RANS zone (zone A): the mesh is kept unchanged.

(ii) In the LES zone (zone C): the new unstructured mesh is built, composed of cells whose local target size is given by Eq (7).

(iii) In the transition zone (zone B): the targeted cell size in the transition zone is equal to the maximum cell size obtained in the LES zone and the smooth transition between the structured RANS and unstructured LES meshes is ensured by the meshing tool.

In this study, the GMSH software [19] is used to generate the grids. The unstructured zones are meshed with the Packing of Parallelograms algorithm. After each computation, the statistically averaged quantities are used to determine the LES region and the local grid requirements for LES for the next one. These instructions are provided to GMSH to generate the grid for the next computation. The interface between the LES and the RANS mode is smoothed to avoid the numerical errors caused by a discontinuity in the targeted energy ratio.

4 Turbulence modeling

Although the self-adaptive methodology can be associated to any continuous hybrid RANS/LES approach, HTLES-$k-\omega$-SST [14] is used in the present study, in its active version recently proposed by Mehta et al. [33]. For more details, the reader is referred to these two papers.

4.1 Hybrid Temporal LES (HTLES)

Derived from the PITM model [8, 16], the HTLES is a continuous hybrid approach in which the hybridization term in the energy equation is based on a time scale driven by the energy ratio r. The equations resolved are the following:

$$\begin{cases} \nu_{\text{sfs}} = \dfrac{a_1 k_{\text{sfs}}}{\max\left[a_1 \psi(r) \omega^*_{\text{sfs}}, F_2 \widetilde{S}\right]}, \\ \dfrac{\partial k_{\text{sfs}}}{\partial t} + \widetilde{U}_k \dfrac{\partial k_{\text{sfs}}}{\partial x_k} = P_{\text{sfs}} + D_{k\text{sfs}} - \dfrac{k_{\text{sfs}}}{T_{\text{m}}}, \\ \dfrac{\partial \omega^*_{\text{sfs}}}{\partial t} + \widetilde{U}_k \dfrac{\partial \omega^*_{\text{sfs}}}{\partial x_k} = \gamma_\omega \dfrac{\omega^*_{\text{sfs}}}{k_{\text{sfs}}} + D^*_{\omega\text{sfs}} \\ \qquad\qquad -\beta_\omega {\omega^*_{\text{sfs}}}^2 + C^*_{\omega\text{sfs}}, \end{cases} \tag{8}$$

with the production limiter

$$P_{\text{sfs}} = \min\left[\nu_{\text{sfs}} \widetilde{S^2}, a_2 C_\mu k_{\text{sfs}} \psi(r) \omega^*_{\text{sfs}}\right], \tag{9}$$

the diffusion terms

$$D_{k\text{sfs}} = \frac{\partial}{\partial x_j}\left[\left(\nu + \frac{\nu_{\text{sfs}}}{\sigma_k}\right)\frac{\partial k^*_{\text{sfs}}}{\partial x_j}\right] \tag{10}$$

and

$$D_{\omega\text{sfs}} = \frac{\partial}{\partial x_j}\left[\left(\nu + \frac{\nu_{\text{sfs}}}{\sigma_\omega}\right)\frac{\partial \omega^*_{\text{sfs}}}{\partial x_j}\right], \tag{11}$$

and the cross-diffusion term,

$$C^*_{\omega\text{sfs}} = (1-F_1)^2 \frac{1}{\sigma_{\omega_2}} \frac{1}{\psi(r)\omega^*_{\text{sfs}}} \frac{\partial \omega^*_{\text{sfs}}}{\partial x_j} \frac{\partial k_{\text{sfs}}}{\partial x_j}. \tag{12}$$

$\beta_\omega = C_\mu(C_{\epsilon 2} - 1)$, $\gamma_\omega = C_{\epsilon 1} - 1$, F_1 and F_2 the blending functions, and a_1, a_2, $C_{\epsilon 1}$, and $C_{\epsilon 2}$ are the usual coefficients of the k-ω SST model.

T_{m} is the turbulent time scale that drives the transition from the RANS mode to the LES mode

$$T_{\text{m}} = \frac{r}{\psi(r)} \frac{k_{\text{m}} + c_r k_r}{C_\mu k_{\text{m}} \omega^*_{\text{m}}}, \tag{13}$$

where c_r is the coefficient imposing the *internal consistency constraint*: in the RANS zone, resolved energy due to the penetration of turbulent structures from the LES region is not counted in the total turbulent energy in order to strictly tend to the RANS model in this zone,

$$c_r = \begin{cases} 0 \text{ if } r = 1, \\ f_s \text{ if } r < 1. \end{cases} \tag{14}$$

$\psi(r)$ is the hybridization function defined by

$$\psi(r) = \frac{\beta_\omega}{C_\mu \gamma_\omega + r(\beta_\omega - C_\mu \gamma_\omega)}. \tag{15}$$

This expression goes to unity when $r = 1$, such that the RANS model is recovered.

The energy ratio

$$r = (1 - f_s) + f_s \times \min\left[1, r_K\right]. \tag{16}$$

Table 1: Coefficients of the HTLES-$k-\omega$-SST model.

β_0	γ	C_1	C_2	p_1	p_2
0.48	2/3	13.5	1.2	8	6

involves the shielding function f_s introduced by Duffal et al. [14] to avoid grid-induced separation and the log-layer mismatch when ambiguous near-wall meshes are used (fine enough to resolve turbulent structures but too coarse to perform wall-resolved LES):

$$f_s = 1 - \tanh\left[\max\left(\xi_K^{p1}, \xi_D^{p2}\right)\right], \tag{17}$$

with $\xi_K = C_1\left(\nu^3/\epsilon\right)^{1/4}/d_w$, and $\xi_D = C_2\Delta_{max}/d_w$, where d_w is the distance to the wall and Δ_{max} the local cell elongation (longest edge of the cell). The energy ratio r_K, active far from the wall where the shielding function goes to one, is obtained analytically from an equilibrium Eulerian temporal spectrum [45],

$$r_K = \frac{1}{\beta_0}\left(\frac{U_s}{\sqrt{k}}\right)^{2/3}\left(\omega_c\frac{k}{\epsilon_m}\right)^{-2/3} \tag{18}$$

where

$$\epsilon_m = C_\mu k_\mathrm{m}\psi(r)\omega_\mathrm{m}^*, \tag{19}$$

$\omega_c = \min\left[\frac{\pi}{dt}, \frac{U_s\pi}{\Delta}\right]$ is the cutoff frequency, $\Delta = \Omega^{1/3}$ with Ω the cell volume, and $U_s = U + \gamma\sqrt{k}$ is the sweeping velocity. Note that in the present study, the time-step is smaller than Δ/U_s everywhere in the domain, such that $\omega_c = U_s\pi/\Delta$ and r_K is given by Eq. 6. The constants used are summarized in Tab. 1 and more details can be found in [14].

As mentioned in Sec. 3.1, the criterion $P/\epsilon > \alpha$ is biased if the resolved part of the dissipation is not taken into account, particularly in the low Reynolds number recirculation region. In order to avoid the cumbersome computation of the resolved part of dissipation during the simulation, Eq. (4) is used, where the modeled-to-total dissipation ratio $r_\epsilon = \epsilon_m/\epsilon$ is evaluated, assuming a Kolmogorov spectrum, from the definition of the energy and dissipation ratios, r and r_ϵ, respectively, and the integration of the energy and dissipation spectra between the integral and the Kolmogorov length scales. Denoting by a hat variables made non-dimensional based on ϵ, k and ν_t, we have

$$r_\epsilon = \frac{\hat{\epsilon}_\mathrm{m}}{\hat{\epsilon}} = \frac{1}{\hat{\epsilon}}\int_{\hat{\kappa}_c}^{\hat{\kappa}_\eta}\frac{2}{R_t}C_\kappa\hat{\kappa}^{1/3}\mathrm{d}\hat{\kappa}, \tag{20}$$

where $R_t = \nu_t/\nu$ is the turbulent Reynolds number, yielding

$$r_\epsilon = 1 - \frac{\pi^2}{\hat{\Delta}^{4/3}R_t}. \tag{21}$$

Similarly, from

$$r = \frac{\hat{k}_\mathrm{m}}{\hat{k}} = \frac{1}{\hat{k}}\int_{\hat{\kappa}_c}^{\hat{\kappa}_\eta}C_\kappa\hat{\kappa}^{-5/3}\mathrm{d}\hat{\kappa}, \tag{22}$$

one can obtain

$$r = \hat{\Delta}^{2/3}\frac{\pi^{2/3}}{R_t^{1/2}}. \tag{23}$$

Combining Eqs. (21) and (23) gives

$$r_\epsilon = 1 - \left(1 + \frac{rR_t^{1/2}}{\pi}\right)^{-2}. \tag{24}$$

Since dissipative scales are smaller than energetic scales, $r_\epsilon \geq r$, such that the final expression is

$$r_\epsilon = \max\left[1 - \left(1 + \frac{C_{r_\epsilon}rR_t^{1/2}}{\pi}\right)^{-2}, r\right]. \tag{25}$$

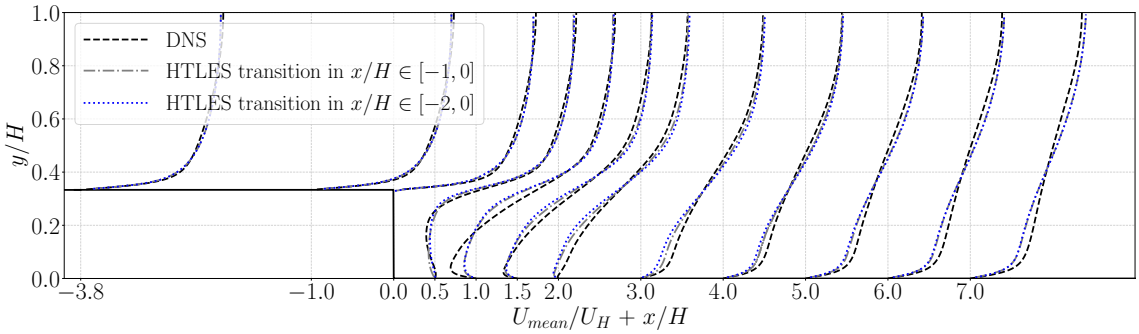

Fig. 6: Streamwise velocity profiles in the y direction for 12 streamwise locations. DNS results are from Lamballais [28].

With this expression, $r_\epsilon = 1$ in the RANS mode since $r = 1$ and goes to zero at the DNS limit where $r = 0$. $C_{r_\epsilon} = 0.42$ is a coefficient calibrated by comparing dissipation fields obtained in hybrid RANS/LES and RANS.

4.2 Active approach

In continuous hybrid RANS/LES, during the transition from RANS mode to LES mode, the modeled turbulent energy is reduced by the model. However, the growth of the resolved energy is slow, leading to a strong local underestimation of the total turbulent energy and the turbulent stresses. To mitigate this gray area issue, Mehta et al. [33] have developed the *active* approach, which injects the proper amount of energy into the resolved motion via a body force in the momentum equation written as

$$f_i = A_{ij}\widetilde{U}_i + B_i, \tag{26}$$

where $\widetilde{U}_i$ is the resolved velocity. A_{ij} and B_i have to satisfy two constraints: (i) energy injection in the resolved scales is imposed by the rate of energy removal in the modeled scales; (ii) the forcing should not affect the mean flow. It can be shown that these constraint are satisfied if A_{ij} and B_i are determined by solving at each point of the domain the system

$$\begin{cases} A_{ik}\overline{u'_j u'_k} + A_{jk}\overline{u'_j u'_k} = -\tau^{\mathrm{m}}_{ij}\dfrac{1}{r}\dfrac{\mathrm{d}r}{\mathrm{d}t}, \\ B_i = -A_{ij}\overline{\widetilde{u}_j}, \end{cases} \tag{27}$$

where u'_i is the fluctuating part of the resolved velocity and $\overline{\cdot}$ stands for the Reynolds average. The force is thus a function of the rate of change of the energy ratio in the flow direction $\mathrm{d}r/\mathrm{d}t$ and goes to zero where the mesh is uniform. This *active* version of the HTLES is used for all the simulations in the present paper.

5 Results and discussion

This section aims to present the results obtained with the self-adaptive strategy. It is organized as follows: in subsection 5.1, the influence of the length of transition from RANS to LES is investigated, in subsection 5.2, the evolution of the LES and transition zones as well as the mesh is commented, and in subsection 5.3, the results are compared with reference data.

5.1 Influence of the length of transition

The transition from RANS to LES induces a loss of total turbulent kinetic energy as explained in Sec. 4. To compensate for this loss, a forcing is added to rapidly generate resolved turbulent structure. The purpose of this subsection is to set the forcing.

The self-adaptive strategy could be applied to any hybrid RANS/LES model. For this feasibility study, we are using the Active HTLES model [33], described in Sec. 4. It is important to remember that the aim of this article is not to evaluate the performance of this particular hybrid RANS/LES model, but to develop a self-adaptive method. In the active HTLES approach, forcing is introduced to generate resolved fluctuations at the entrance of the LES region. The intensity of the fluctuating body force added to the momentum equation is determined by Eq. (27) and relies on the material derivative of the energy ratio r. Thus, increasing the length l_{inl} of the RANS-to-LES transition upstream the step corner (Fig. 5) has different and contradictory consequences. On the one hand, since the refinement of the mesh in the flow direction is less rapid, the energy ratio $r = k_m/k$ decreases more slowly and the intensity of the forcing is reduced. On the other hand, the resolved structures have more space for developing, since the force is active over a longer region. The influence of l_{inl} is in theory moderate, since these two effects compensate for each other: $(1/r) \times \mathrm{d}r/\mathrm{d}t \simeq (1/r) \times U\partial r/\partial x$ is of the order of U/l_{inl}, where U is the streamwise mean velocity, and since the distance travelled is l_{inl}, the work done by the force is globally independent of l_{inl}.

However, Mehta et al. [33] showed, in the case of a channel flow, that the realistic turbulent structures cannot develop if the transition region is too short. Therefore, a preliminary study is performed here to determine the value of C_{inl} to be used in Eq. (5).

In this preliminary study, a structured mesh of 5.7M cells is used, which is fine enough to be in LES mode everywhere. However, the RANS mode is artificially imposed in the inlet channel, as well as a transition in the region $x \in [x_{\mathrm{trans}}; 0]$ upstream of the step. To achieve this, the energy ratio r related to the grid step given by Eqs. (16) and (18) is modified by imposing $r_{\mathrm{mod}} = 1$ in the inlet channel up to the position $x = x_{\mathrm{trans}}$ and then a gradual decrease of the form

$$r_{\mathrm{mod}} = f + (1 - f)r \quad \text{with} \quad f(x) = \frac{x}{x_{\mathrm{trans}}}, \tag{28}$$

such that the usual value of r is recovered at the step corner ($x = 0$). In Fig. 6, the streamwise velocity profiles are presented for two different cases, $x_{\mathrm{trans}}/H = -1$ and $x_{\mathrm{trans}/H} = -2$. The profiles are nearly superimposed, showing that $x_{\mathrm{trans}}/H = -1$ is sufficient. Reducing further the transition zone does not allow to generate realistic structures (not shown here): when the forcing is too intense, the fluctuations generated, which are solution of the forced momentum equations, no longer resemble turbulent structures, and are then dissipated when the forcing stops. This is in agreement with the observations of Druault et al. [12]. The transition zone has to be long enough so that the forcing term is not too strong compared to the other terms of the resolved momentum equation at the end from the transition zone. Since a slightly better agreement with DNS is found for the case with the shorter transition length, and with the purpose of reducing the global cost of the computations, this order of magnitude of $l_{inl}/H \approx 1$ is retained for building the zone B (see Fig. 5). Based on the RANS results, this approximately correspond to calibrating the constant in Eq. (5) as $C_{inl} = 5$.

5.2 Evolution of the zones and the mesh

The region where switching to LES mode is desirable is obtained from Eq. (2), using $\alpha = 1.4$. The cell size to reach the targeted energy ratio r is given by Eq. (7). The targeted value $r = 0.1$ is used, except for the first iteration, called HTLES1 below, for which the less strict value $r = 0.15$ is applied to save computational time, since it is only the first mesh determined by the probably inaccurate RANS results. Note that our objective here is not to design a mesh corresponding to well-resolved LES. Indeed, the ratio r appears in the analytical derivation of the HTLES model (as well as in other models, such as PITM or PANS), as driving the changeover from RANS to LES. Therefore, designing a mesh corresponding to a small value of r simply ensures that the model switches to LES mode at the next iteration of the algorithm. If one wants to make sure that a well-resolved LES is performed, it is straightforward to additionally introduce relevant criteria available in the literature. The mesh and zone obtained for the successive computations are

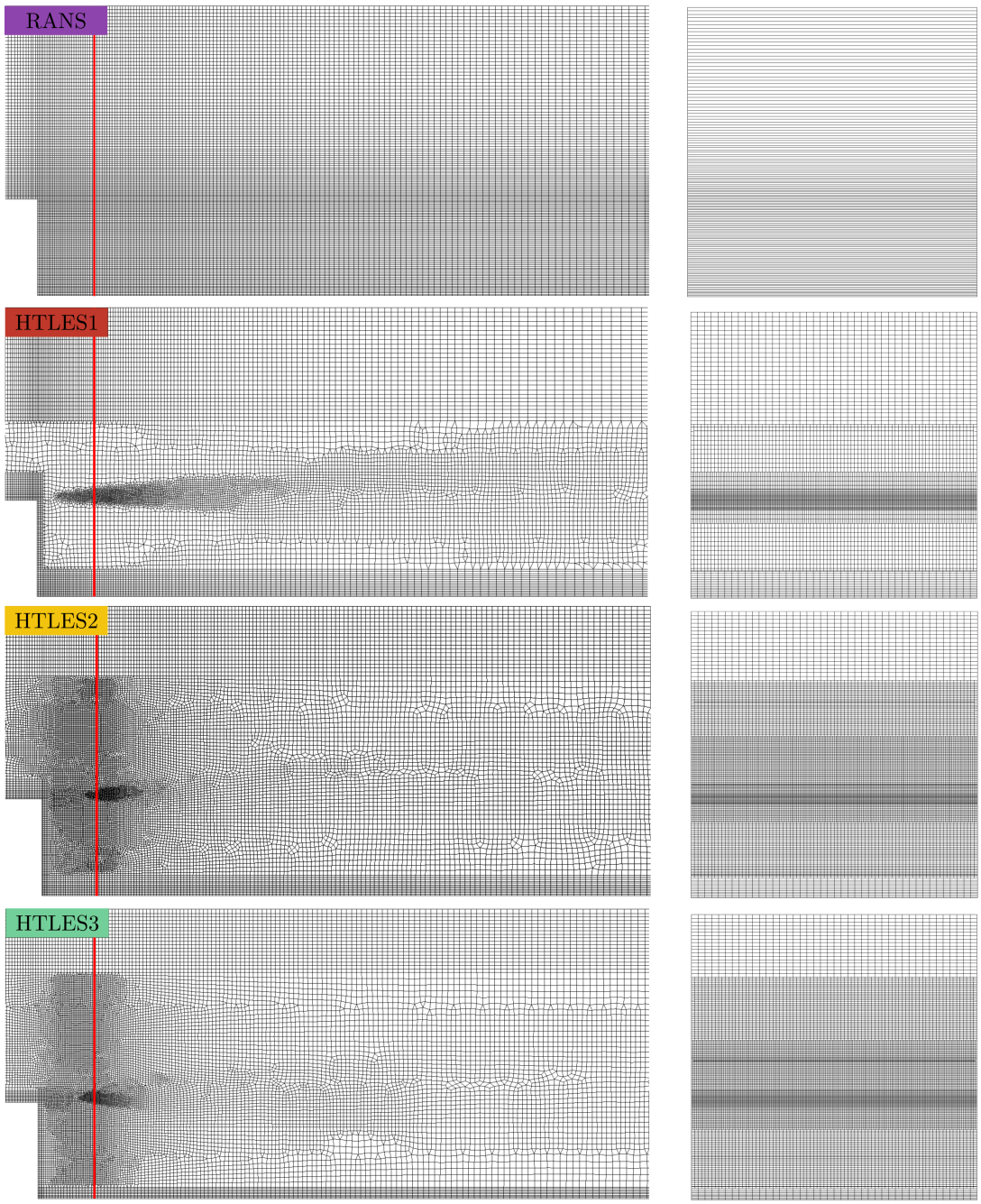

Fig. 7: Visualization of the mesh for the RANS, HTLES1, HTLES2, and HTLES3 computations. The red line on the mesh view corresponds to the plane $x/H = 0.2$. On the right side, the mesh in this plane is displayed. HTLES1, HTLES2, and HTLES3, respectively correspond to the first, second, and third HTLES in the sequence of performed computations.

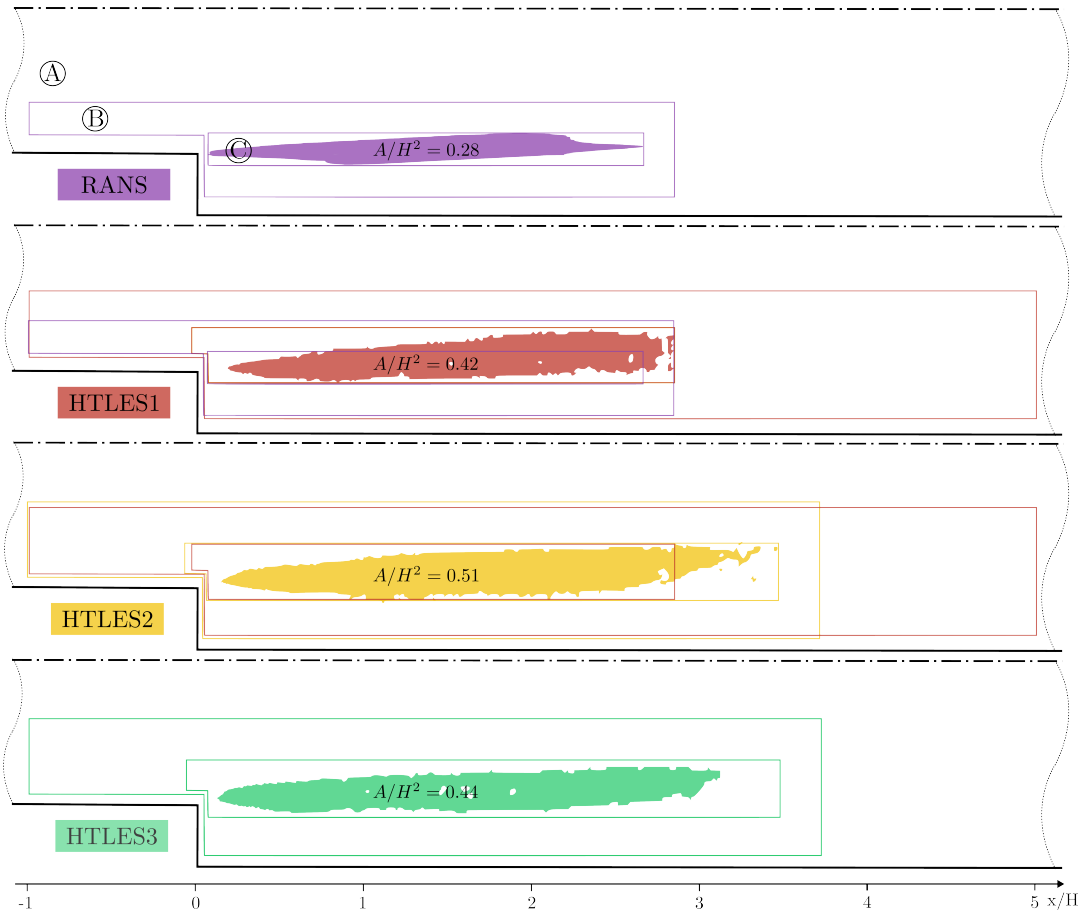

Fig. 8: Visualization of the different zones for the RANS, HTLES1, HTLES2, and HTLES3 computations. The values of A/H^2 indicated are the non-dimensional area of the region identified by the criterion. HTLES1, HTLES2, and HTLES3, respectively correspond to the first, second, and third HTLES in the sequence of performed computations.

Table 2: Grid characteristics. The number of cells is divided by 10^6.

	RANS	HTLES1	HTLES2	HTLES3
N	0.10	2.21	3.37	3.09
$N_{LES+transi}$	0	1.13	2.45	2.23
N_{LES}	0	0.75	1.27	1.35

presented in Figs. 7 and 8, respectively. The grid characteristics are presented in Table 2. N, $N_{LES+transi}$, and N_{LES} correspond to the number of cells in the domain, the LES and transition regions, and the LES region, respectively.

A RANS computation, performed on a fully structured grid composed of 95 800 cells obtained after a grid convergence study, is used to initialize the algorithm. Note that the mesh consists of only one cell in the z direction due to spanwise periodicity. The methodology is designed to mitigate initial RANS errors by iteratively performing hybrid RANS/LES computations until a stable point is achieved. Nonetheless, it is important to note that RANS results provide the boundary conditions for the LES zone, highlighting the necessity of improving RANS modeling. Since the method aims to switch to LES when RANS is no longer efficient, it can be assumed that where RANS is used, it provides sufficiently accurate results to support the LES zone. Following the rules presented in Sec. 3.2, the region corresponding to $P/\epsilon > \alpha$ is extracted and used to determine the boundaries of the LES and transition zones of the first HTLES

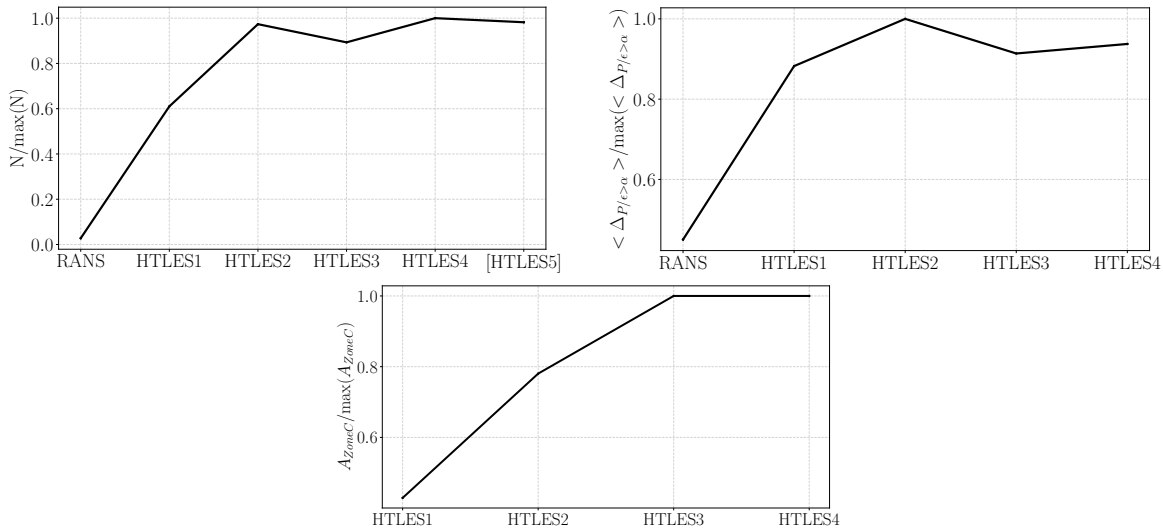

Fig. 9: Top: number of cells and averaged value of Δ in the region where $P/\epsilon > \alpha$. Bottom: area of Zone C. All the quantities are normalized by the maximum value of the data series. Note that HTLES5 has not been run, but the mesh, built with the results of HTLES4, is displayed to highlight the fixed point reached by the algorithm. HTLES1, HTLES2, and HTLES3, respectively correspond to the first, second, and third HTLES in the sequence of performed computations.

computation (purple boxes). The cell size in the LES region is computed following the rules described in Sec. 3.3. The HTLES1 mesh is generated by GMSH according to these zones and cell size requirements. In the HTLES computations, the grids in the transition and LES zones are also refined in the z-direction to obtain cells which are as isotropic as possible. The HTLES1 computation is then performed and the region corresponding to $P/\epsilon > \alpha$ is updated based on the time-averaged results. Here, it extends until the end of the transition zone thus, following the rules established in Sec. 3.2, the thickness of the transition zone utilized for HTLES2 (largest red box in Fig. 8) is increased in this direction to mitigate the total number of algorithm iterations. The same procedure is repeated for HTLES2 and HTLES3 (Fig. 8). The results of HTLES3 show that the area of the LES zone is reduced when compared to the one of HTLES2. This meets the stopping criterion presented in Fig. 2. Specifically, if at the end of a computation, the area of the LES zone is reduced when compared to the one of the previous one, the process is stopped. Thus the algorithm is stopped since the LES region is sufficiently large, and trying to optimize its size would lead to extra iterations of the algorithm that would actually increase the total computational cost. Here, we still performed a fourth HTLES run, using the same zones but cell sizes computed from HTLES3 results, to confirm that the algorithm has reached a fixed point.

The cell number, the averaged value of Δ, the cell size to reach the targeted energy ratio in the region where the criterion (2) is satisfied and the area of zone C are shown in Fig. 9. Except for HTLES2 whose transition zone size has been increased, as explained above, to reduce the total number of algorithm iterations, the grid size exhibits a monotonic increase from RANS to HTLES4. The mesh obtained after the computation of HTLES4, which would have been used for HTLES5 if the algorithm were not stopped, is reduced when compared to the one obtained after HTLES3, highlighting the stabilization of the method. After a monotonic increase, the normalized value $\langle\Delta\rangle_{P/\epsilon>\alpha}/max\left(\langle\Delta\rangle_{P/\epsilon>\alpha}\right)$ obtained with HTLES3 is reduced when compared to HTLES2, and remains virtually constant between HTLES3 and HTLES4. A similar behavior is observed in the graph showing the area of Zone C reaching a plateau. From these graphs, it is clear that the proposed method reaches a fixed point. The cell number, the averaged value of Δ, the cell size to reach the targeted energy ratio in the region where the criterion (2) is satisfied and the area of zone C are shown in Fig. 9. Except for HTLES2 whose transition zone size has been increased, as explained above, to reduce the total number of algorithm iterations, the grid size exhibits a monotonic increase from RANS to HTLES4. The mesh obtained after the computation of HTLES4, which would have been

used for HTLES5 if the algorithm were not stopped, is reduced when compared to the one obtained after HTLES3, highlighting the stabilization of the method. After a monotonic increase, the normalized value $\langle \Delta \rangle_{P/\epsilon>\alpha} / max\left(\langle \Delta \rangle_{P/\epsilon>\alpha}\right)$ obtained with HTLES3 is reduced when compared to HTLES2, and remains virtually constant between HTLES3 and HTLES4. A similar behavior is observed in the graph showing the area of Zone C reaching a plateau. From these graphs, it is clear that the proposed method reaches a stable solution. The method relies on a sequence of hybrid RANS/LES computations, thus the question of its relevancy and the comparison with the computational cost associated with LES arises. The comparison of the sequence of hybrid RANS/LES computation with one single LES would not be fair because when performing a LES study it is necessary to carry out at least three computations to assess the grid influence. For this reason, the number of computations to be performed for a LES study of an industrial test case or with the self-adaptive strategy is similar, nonetheless, since in hybrid RANS/LES a significant part of the computational domain is in RANS, the total number of grid points and thus the computational cost are expected to be lower with the proposed approach. This is amplified if the computations are restarted from one to another.

5.3 Comparison with DNS

In this section the results obtained after the different iterations of the algorithm are compared with DNS. The results of HTLES4 computation are not shown since they are virtually superimposed with those of HTLES3.

In Fig. 10, the targeted energy ratio (i.e., used in the model, given by Eq. (16)), the effective energy ratio (i.e., the ratio of modeled to total turbulent energy computed during the simulation), the streamwise velocity, and the turbulent kinetic energy profiles are plotted. Since the DNS and RANS energy ratios are zero and one, respectively, throughout the entire domain, they are not shown. The HTLES energy ratio profiles provide information on the local resolution of the computation and depict the interface between RANS and LES regions. For example, when the target ratio is $r = 0.1$, the model coefficients (see Sec. 4) are adapted to switch to LES mode, aiming for a resolved energy share of 90%. The effective ratio r_{eff}, on the other hand, measures during the calculation whether or not this target is actually achieved. Thus, by plotting the profiles of these two ratios in the domain, we can visualize how the zone in which the model and simulation switch to LES mode evolves over the iterations of the algorithm. The area of the LES region significantly increases from HTLES1 to HTLES2, and then stabilizes. The effective energy ratio profiles (Fig. 10b) globally follow those of the energy ratio even if some discrepancies appear, reflecting the fact that the partition of energy approximately reaches the expected level. In agreement with previous studies (Duffal et al. [14]), the effective ratio corresponds well to the target ratio in the heart of the LES zone, but the most critical areas are the rapid transition zones, where the response of the simulation (measured by the effective ratio) is not as sharp as the variations in the target ratio. In particular, this issue is critical upstream of the LES zone, in the transition region from RANS to LES, which motivated the development of volume forcing by Mehta et al. [33] that is used here and succeeds quite well in generating resolved energy rapidly. The results indicate that downstream of the LES region, some resolved scales penetrate the RANS region. Mehta et al. [33] made the same observation for the case of a periodic hill, and concluded that it was not a problem, since their results are actually better than pure RANS results. Note that close to the wall, the effective energy ratio is not relevant since both k_m and k_r go to zero. The effective energy ratio decreases near the wall in front of the step because both the modeled and resolved turbulent kinetic energies approach zero at the wall, resulting in $r_{eff} \approx 0/0$. This behavior is also observed downstream of the step. Upstream, at $x/H = -3.8$ and $x/H = -1$, there are no resolved structures since the RANS mode is activated, thus, the resolved turbulent kinetic energy is exactly zero. Meanwhile, the modeled part decreases as it gets closer to the wall, leading to $r_{eff} = 1$. The spikes in the profiles are due to the sharp variations of the total turbulent kinetic energy (Fig. 10d).

Regarding the streamwise velocity (Fig. 10c), upstream the transition region, the RANS mode is imposed and periodic RANS solution imposed at the inlet is preserved. The mesh refinement from $r = 0.15$ (HTLES1) to $r = 0.10$ (others) in the LES region and the definition of the zones has little influence on the streamwise velocity and turbulent kinetic energy (Fig. 10d) profiles, which highlights the robustness of the method. The expansion of the LES zone in the recovery region (HTLES2 and HTLES3) improves the turbulent kinetic

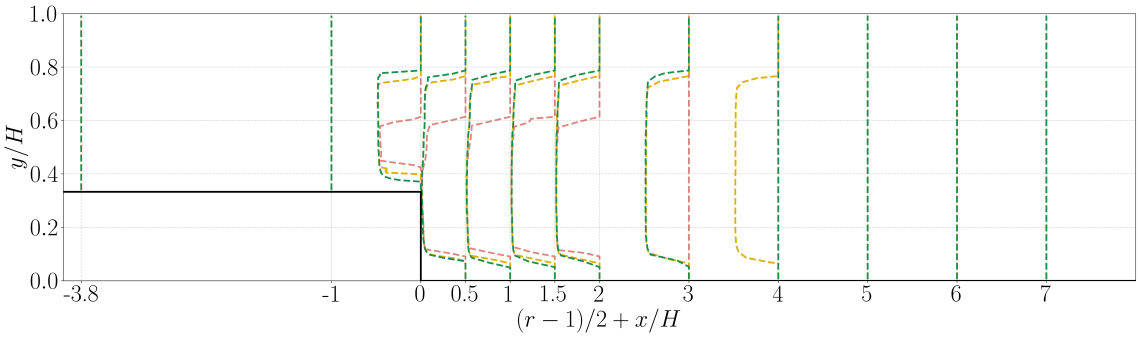

(a) Targeted energy ratio (used in the equations of the model, given by Eq. (16))

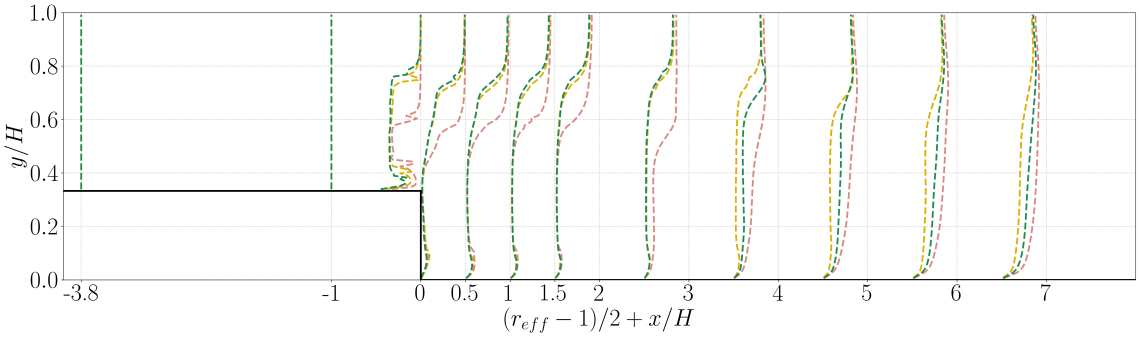

(b) Effective energy ratio (ratio of modeled to total turbulent energy measured during the computation)

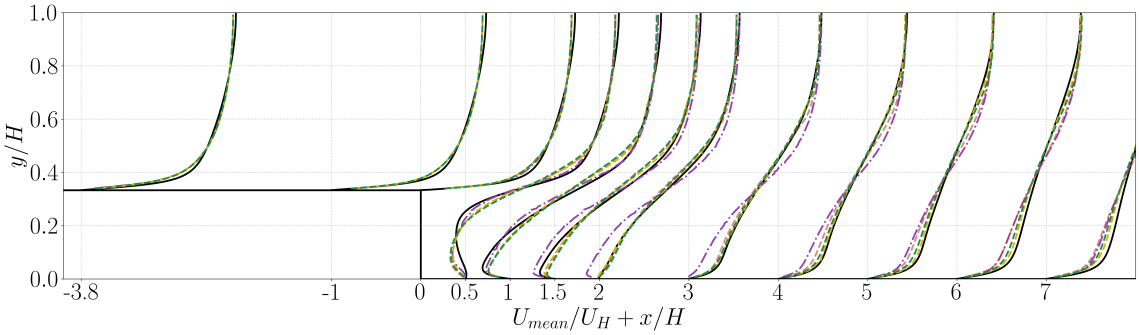

(c) Streamwise velocity

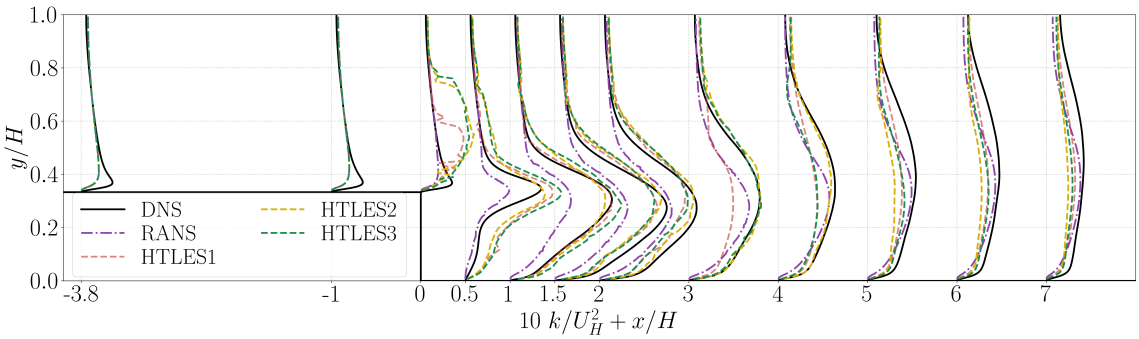

(d) Total turbulent kinetic energy

Fig. 10: Profiles in the y-direction for 12 streamwise locations. DNS results are from Lamballais [28]. HTLES1, HTLES2, and HTLES3, respectively correspond to the first, second, and third HTLES in the sequence of performed computations.

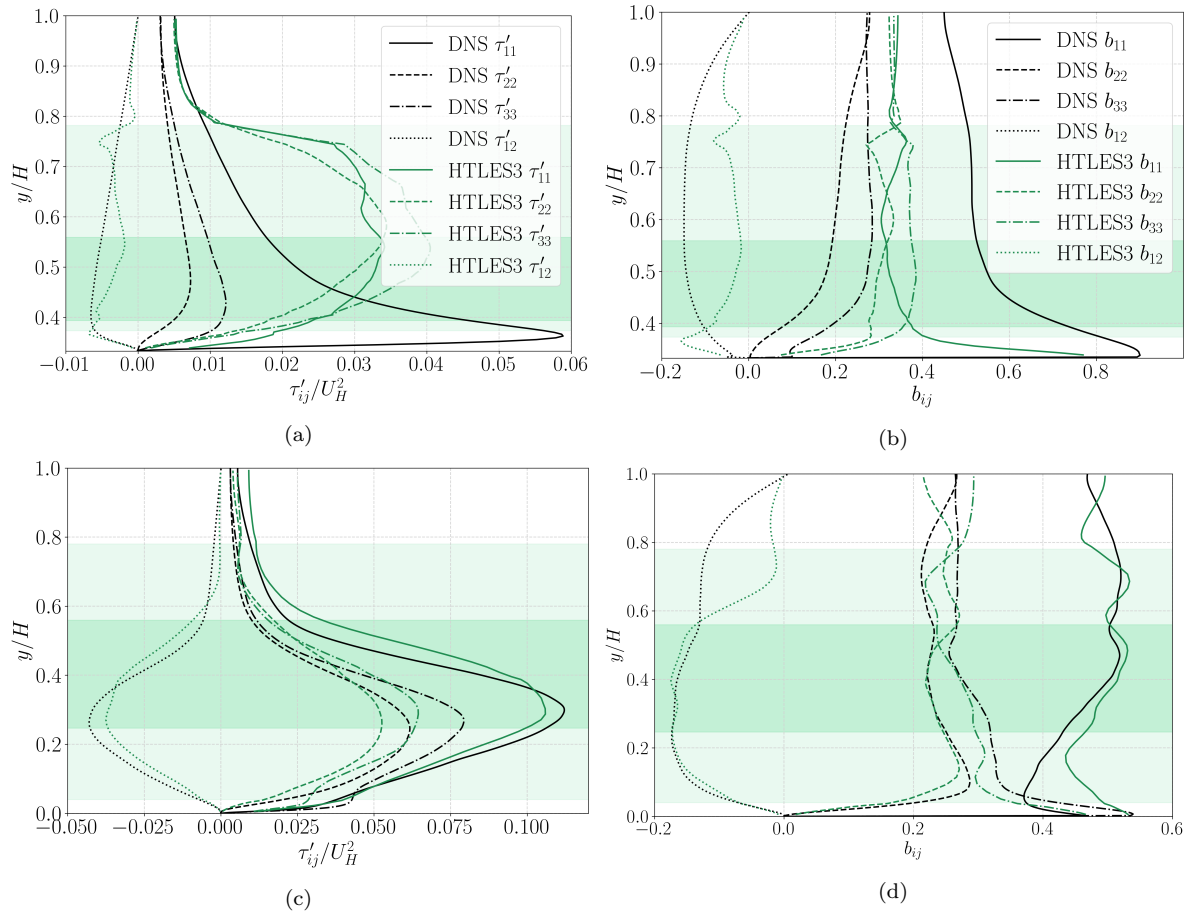

Fig. 11: Profiles of the Reynolds stresses (left) and anisotropy components (right) in the y direction for $x/H = 0$ (top) and $x/H = 1.5$ (bottom). The white, light green and medium green zones show the RANS, transition, and LES zones, respectively. DNS results are from Lamballais [28].

energy profiles at $x/H = 3$ and, for HTLES2, which has the largest LES zone, until $x/H = 4$. The spikes of turbulent kinetic energy, principally observed at $x/H = 0$, are due to the rapid RANS/LES transition in the vertical direction and to the forcing term that depends on the variations of the energy ratio. The overshoot of turbulent kinetic energy observed near the step in all HTLES rapidly fades out. This is due to the forcing term, as observed by Mehta et al. [33] for channel and periodic hill flows. The forcing generates structures which are solution of the forced momentum equations. When leaving the forcing zone, some of the energy of these structures is dissipated, because they are not exact solutions of the unforced momentum equations. It is therefore beneficial to have an energy overshoot on leaving the forcing zone. Comparing RANS with HTLES3, it appears that RANS significantly underestimates the amount of turbulent kinetic energy from $x/H = 0$ to $x/H = 2$, while it is well estimated by the HTLES3. A close agreement with DNS is found between $x/H = 1$ and $x/H = 3$, which makes possible an accurate prediction of the streamwise velocity profiles between $x/H = 2$ and $x/H = 4$. Downstream of the location $x/H = 4$, the HTLES streamwise velocity profiles are slightly improved when compared to the RANS profiles.

The total Reynolds stresses, $\tau'_{ij} = (\overline{u_i u_j} - \overline{u}_i \overline{u}_j) + \tau^{\mathrm{m}}_{ij}$, and the corresponding anisotropy components, defined as

$$b_{ij} = \frac{\tau'_{ij}}{2k} - \frac{1}{3}\delta_{ij}, \tag{29}$$

are shown in Fig. 11 for HTLES3, at the streamwise locations $x/H = 0$ (top) and $x/H = 1.5$ (bottom). The white, light green and medium green zones show the RANS, transition, and LES zones, respectively.

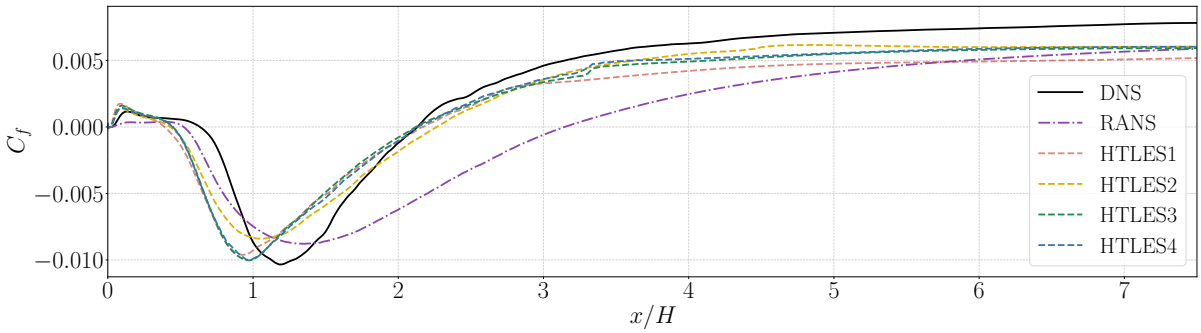

Fig. 12: Distribution of skin friction on the wall downstream of the step. DNS results are from Lamballais [28]. HTLES1, HTLES2, and HTLES3, respectively correspond to the first, second, and third HTLES in the sequence of performed computations.

Figs. 11a and 11b show that the fluctuations generated by the forcing do not exhibit the correct anisotropy upstream of the step. This is explained because the volumic forcing acts as an amplifier of the preexisting fluctuations based on Eq. (27), in which τ_{ij}^{m} is the anisotropy tensor given by the linear eddy viscosity models. Correct anisotropy could only be obtained if the RANS model itself was capable of representing it, as with a Reynolds-stress model or an explicit algebraic stress model. Nonetheless, the cross component τ'_{12}, which is the most significant in the computation of the energy production term, is well approximated. At $x/H = 1.5$, the Reynolds stresses is quite well predicted, specifically for the τ'_{11} and τ'_{12} components. In Fig. 11d, despite the poor prediction of the anisotropy in $x/H = 0$, the results observed in the LES region are remarkably close to those of the DNS.

The skin friction distribution on the lower wall, shown in Fig. 12, highlights the benefits associated with the self-adaptive method. Indeed, the HTLES3 profile leads to a relatively correct prediction of the negative peak of C_f and gives a very accurate estimate of the reattachment location. Note that the results of HTLES1, which mesh is significantly coarser than that of HTLES3 in the transition and LES regions (see Fig. 7), are quite accurate, underlying the robustness of the HTLES to mesh coarsening. HTLES gives remarkably better results than RANS in the recirculation zone and downstream of it. Moreover, the peak of C_f observed in DNS at $x/H \approx 0.1$, associated with the secondary counterclockwise recirculation zone, is well reproduced by HTLES while it is not predicted by RANS. The kinks in the C_f profiles at $x/H = 3.3$ are explained by the sharp transition from LES to RANS. Far in the recovery region, HTLES tends toward RANS profiles since the RANS mode is reactivated. The computations HTLES3 and HTLES4 are almost superimposed, emphasizing the stabilization of the self-adaptive strategy around a relevant hybrid RANS/LES solution, improved when compared to RANS, HTLES1, and HTLES2, and achievable in industry. It is worth emphasizing that, overall, the HTLES1 computation, carried out with a targeted energy ratio of 0.15, which corresponds to a quite poorly resolved LES, still gives relatively good results. This highlights the robustness of the self-adaptive strategy applied with the HTLES and its applicability with relatively coarse LES mesh. Despite the fact the Reynolds number of the present case is low, this robustness to coarse meshes suggests that the methodology can be expected to be applicable to industrial flows at high Reynolds number.

Mean streamlines computed using the line integral convolution (LIC) are displayed in Fig. 13. The two classically observed recirculation zones [10] are visible. The main recirculation zone (clockwise) extends up to $x/H = 2.1$ and the secondary recirculation zone (counterclockwise) to $x/H = 0.4$, to be compared to the DNS values, $x/H = 2.13$ and $x/H = 0.63$, respectively.

Fig. 14 shows the Q-isocontours obtained with HTLES3, with the intention of showing qualitatively how turbulent structures appear when the ratio r (shown in the background) driving the transition from RANS to LES is less than unity. The figure shows that the active HTLES rapidly develops resolved scales, thanks to the volume forcing. Indeed, turbulent structures are remarkably observed right from the beginning of the LES region. However, downstream of the LES region, the structures are advected into the RANS zone and are only gradually dissipated by the RANS eddy viscosity. As can be seen in Fig. 12, the solution transitions in this region from a LES to a RANS behavior.

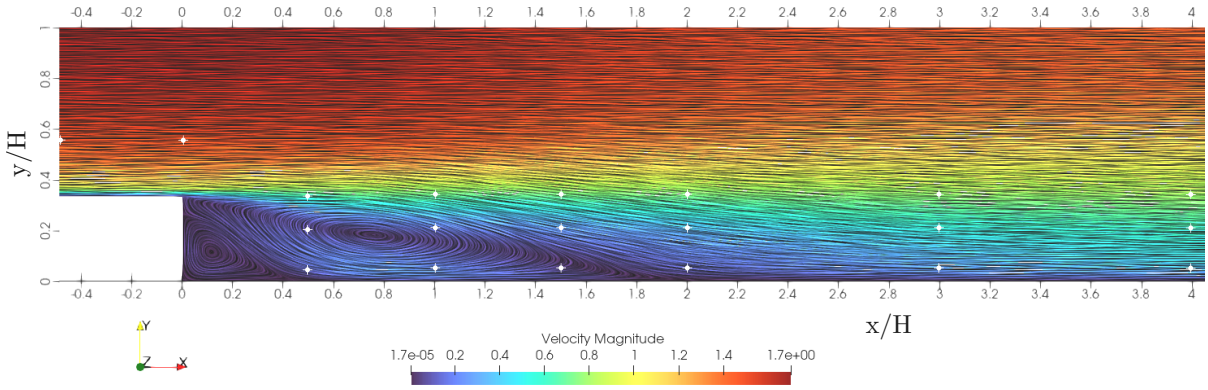

Fig. 13: Mean streamlines of the HTLES3 colored with velocity magnitude. The locations of the probes in the streamwise direction are $x/H = -0.5$, $x/H = 0$, $x/H = 0.5$, $x/H = 1$, $x/H = 1.5$, $x/H = 2$, $x/H = 3$, $x/H = 4$.

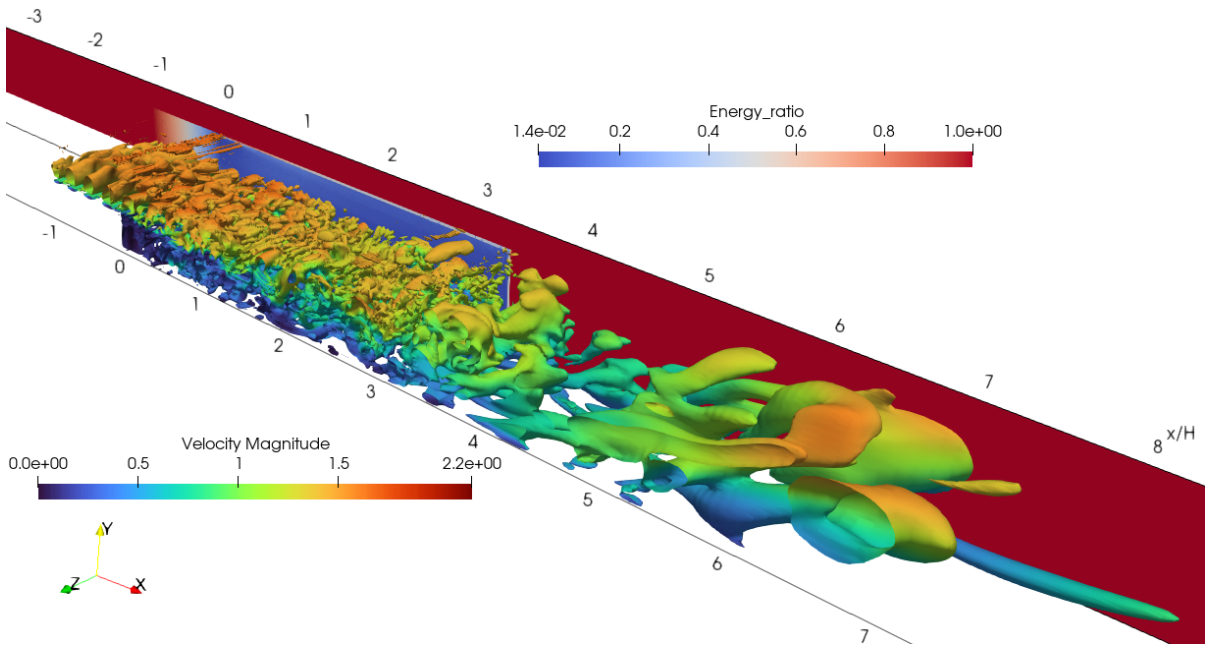

Fig. 14: Q-isosurfaces colored by the velocity magnitude ($Q = 0.5U_H^2/H^2$) and targeted turbulent energy ratio for the HTLES3.

6 Conclusions and future work

In this paper, a demonstrator of a self-adaptive strategy is investigated to mitigate the influence of the user on the results of hybrid RANS/LES computations. Rather than aspiring to outperform expert solutions, the proposed strategy seeks to achieve a stable, relevant, user-independent, and computationally feasible solution within an industrial context. In its final version, the various parameters and criteria will be fixed ensuring the simplicity of the method for users. Since it is still in the ongoing development phase, this is not fully achieved for now but this feasibility study shows encouraging results and paves the way for the future development of this agile strategy.

To avoid the definition of the RANS and LES zones by the user choices made at the time of the construction of the mesh, the zones where to switch to LES are determined by physical criteria, and the

mesh is also refined in this zone to target a resolution obtained based on a physical criterion. The method is assessed on a backward-facing step. For this feasibility study, the proposed strategy is applied with the HTLES-$k-\omega$-SST model. It is crucial to emphasize that this strategy is applicable to any other continuous hybrid RANS/LES model and offers a framework that guarantees the objectivity of results obtained with continuous hybrid RANS/LES models.

Several possible physical criteria within the context of self-adaptive hybrid RANS/LES are investigated and the P/ϵ criterion, which assesses the turbulence equilibrium, is selected for this test case. Starting from a RANS computation for initialization, successive HTLES are carried out using the results of the previous computation to generate the mesh of the next simulation.

The outcomes of the study show that the self-adaptive strategy reaches a fixed point in four iterations. Thus, the cost of the self-adaptive method is similar to that of the conventional method, for which simulations are carried out on several meshes before any conclusions can be drawn. Moreover, since hybrid RANS/LES can lead to a drastic reduction of the number of cells compared to LES, due to the use of RANS in large regions of the domain and close to the wall [46, 14], the method remains a good candidate for industrial applications. The statistically-averaged profiles and the friction coefficient are significantly improved when compared to the RANS computation and are in good agreement with the reference DNS results.

The proposed algorithm is a global framework in which any continuous hybrid RANS/LES model can be utilized. Although many parameters can be adjusted and/or generalized, this first study demonstrates that a self-adaptive strategy can be used effectively. Although using the single criterion based on P/ε was shown sufficient in the particular case of the backward-facing step, a combination of several physical criteria will be necessary in the future. To address real-life flows such as those around wind turbines, full car including open windows, or the undercarriage of an airplane, the present methodology must be capable of handling a variety of flow conditions, such as separated flows and reattachment issues, inherently unsteady flows, complex geometries, and flows with significant heat transfer. Achieving this requires the methodology to be multi-physics and multi-criteria, thus, it need to be assessed and generalized to various industrial flows. The method must employ a combination of criteria to detect modeling errors in RANS, as initiated in Fig. 3, across various types of flows. This process necessitates reference data to determine, either manually or through machine learning, where to transition to LES. Once the LES region is determined, the cell size is automatically given by the targeted energy ratio, or could be combined with criteria based on the evaluation of numerical errors. The choice of the targeted energy ratio (i.e., the mesh resolution in the LES region) and the threshold to trigger the switching to LES can be adapted by experts in each engineering domain, leading to user-independent computations. In addition to the efforts related to the development of a multi-criteria and multi-physics self-adaptive strategy, work has to be carried out to address time-dependent flows. This can be done by replacing the Reynolds average with filtering over a short period of time that is adapted to the flow characteristics. It will result in adapting the LES region and the grid during the computation, making the self-adaptive strategy relevant for time-dependent flows.

As for any new methodology, a great deal of work is still required to make it sufficiently general and applicable without modification to a large number of different configurations. Although the present test case is a relativily low Reynolds number, we are confident regarding the applicability of the methodology to higher Reynolds numbers. Indeed, the main ingredients used in the proposed algorithm are weakly dependent on the Reynolds number. The zones detected by the P/ϵ criterion are the out-of-equilibrium regions that depend essentially on boundary layer perturbations due to pressure gradients, separation, deviations in streamlines due to geometry, *etc.*; the size of the transition zone between the RANS zone and the LES zone (section 3.2) is determined as a function of the integral scale of turbulence, which is virtually independent of the Reynolds number; automatic mesh refinement is set so that a certain proportion of the turbulent energy is resolved (section 3.3): this criterion is hardly sensitive to the Reynolds number and is even asymptotically independent of it [25]. Thus, it is expected that increasing the Reynolds number for the same configuration, such as the backward-facing step, will have very little effect on the algorithm's functioning.

As the algorithm is initialized from a RANS calculation, the user's influence on the results is reduced to the same level as for a RANS calculation. The user's subjective choices, based on intuition and a priori knowledge of the flow physics, may lead to very different zones being defined depending on the user, as illustrated in Fig. 1. Obviously, the criteria used in the self-adaptive algorithm have a definite influence on

the results, but if these criteria are fixed by the developers and not by each user, the results are reproducible and independent of the user, which is of great importance for industrial applications.

Since the method has been developed on a specific flow, future work must be devoted to the application of the self-adaptive strategy to other test cases involving new flow features. With the aim of developing a robust methodology useful for a wide range of applications, additional physical criteria will probably be required to locate the zones of interest.

Acknowledgments

This study was funded by E2S UPPA (ANR-16-IDEX-0002) and INRIA in the framework of the ASTURIES project (grant E2S-20-ScientificChallenges-01). The computing resources were provided by MCIA (Mésocentre de Calcul Intensif Aquitain) and GENCI-IDRIS (Grants 2022-A0122A10980 and 2023-A0142A10980).

Ethic declaration

– Funding: E2S UPPA (ANR-16-IDEX-0002) and INRIA-ASTURIES project (grant E2S-20-ScientificChallenges-01)
– Conflict of Interest: the authors declare that they have no Conflict of interest.
– Ethical approval: N/A
– Informed consent: N/A
– Author contribution:
  – Martin David: Methodology; Software; Investigation; Visualization; Writing/Original Draft Preparation
  – Mahitosh Mehta: Investigation; Visualization; Reviewing
  – Rémi Manceau: Conceptualization; Methodology; Supervision; Writing/Review & Editing; Funding Acquisition; Project Administration
– Data Availability Statement: dataset can be made available from the corresponding authors upon request.

Appendix

A Power spectral densities

The Power Spectral Densities (PSD) are computed from instantaneous velocity saved every time step, $\mathrm{d}t = 0.0012$ second, during 165 seconds of simulations, resulting in 137 500 instants. For each streamwise location, monitoring points are saved at nine evenly spaced locations in the periodic direction. The data are concatenated leading to a sample size of $N = 1\,237\,500$ velocities for each PSD. The results are smoothed to improve the readability of the figures. The power spectral densities are defined by

$$\int_0^{+\infty} E(\omega)\mathrm{d}\omega = k. \tag{30}$$

In Fig. 15, the PSD reflect the influence of the forcing on the flow, aiming to rapidly develop turbulence structures to compensate for the decrease of the modeled turbulent energy. The peaks observed for $\omega > 3$ Hz highlight the effect of the forcing on the relatively high-frequency structures while the range corresponding to $\omega < 3$ Hz is not affected. Note that a Strouhal number of 0.1 is found which is in agreement with the study of Celenligil and Mellor [7]. The inertial range is scaled with the classical $-5/3$ slope. Because of its lower energy ratio, the probe located at $x/H = 0$ shows a higher amplitude of the PSD and the sharp decay of the spectrum occurs for higher frequencies than that of $x/H = -0.5$.

The PSD computed downstream of the step are plotted in Fig. 16. In the region of the downstream sensors, the forcing is virtually null since the variations of the energy ratio are low. Hence, contrary the probes located in the forcing region, the PSD decrease monotonously from the inertial to the dissipation ranges. The closer to the wall, the lower the amplitude of the spectra, which is in agreement with the total turbulent kinetic energy profiles. In the inertial range, the $-5/3$ slope is well reproduced for the three y^+ locations. In the high-frequency region, the dissipation scale plays a major role, inducing a fast decay of the turbulent spectrum. The sharp decreases of the slope for very high frequency should not be analyzed since it is beyond the cutoff frequency (colored in light gray). Overall, the PSD express the physical consistency of the turbulent structures generated in the LES region. At $x/H = 4$, the RANS mode is activated and the resolved energy is reduced. The turbulent structures are thus partially filtered out which explains the lower PSD amplitude and the sharper slope in the decay region when compared to the other locations.

References

[1] A. H. Afailal. "Numerical Simulation of Non-Reactive Aerodynamics in Internal Combustion Engines Using a Hybrid RANS/LES Approach". These de Doctorat. Pau, Dec. 2020.

[2] A. H. Afailal, J. Galpin, A. Velghe, and R. Manceau. "Development and validation of a hybrid temporal LES model in the perspective of applications to internal combustion engines". In: *Oil Gas Sci. Technol.* 74.56 (2019), p. 16.

[3] F. Alauzet and L. Frazza. "Feature-based and goal-oriented anisotropic mesh adaptation for RANS applications in aeronautics and aerospace". In: *J. Comput. Phys.* 439 (2021), p. 110340.

[4] F. Archambeau, N. Méchitoua, and M. Sakiz. "Code Saturne: A Finite Volume Code for the Computation of Turbulent Incompressible Flows - Industrial Applications". In: *International Journal on Finite Volumes* 1.1 (2004), http://www.latp.univ.

[5] E. Baglietto, G. Lenci, and D. Concu. "STRUCT : A second-generation URANS approach for effective design of advanced systems". In: *Proc. ASME 2017 Fluids Eng. Division Summer Meeting, FEDSM2017, Waikoloa, Hawaii, USA*. 2017.

[6] R. H. Bush, T. Chyczewski, K. Duraisamy, B. Eisfeld, C. L. Rumsey, and B. R. Smith. "Recommendations for Future Efforts in RANS Modeling and Simulation". In: *AIAA SciTech 2019 Forum*. San Diego,CA, Jan. 2019.

[7] M. C. Celenligil and G. L. Mellor. "Numerical Solution of Two-Dimensional Turbulent Separated Flows Using a Reynolds Stress Closure Model". In: *Journal of Fluids Engineering* 107.4 (Dec. 1985), pp. 467–476. ISSN: 0098-2202.

[8] B. Chaouat and R. Schiestel. "A New Partially Integrated Transport Model for Subgrid-Scale Stresses and Dissipation Rate for Turbulent Developing Flows". In: *Physics of Fluids* 17.065106 (2005), pp. 1–19.

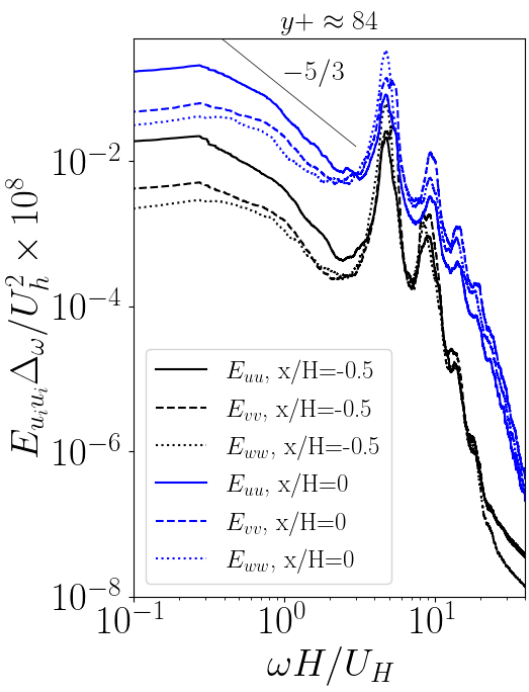

Fig. 15: Power spectral densities of the streamwise, wall-normal, and spanwise velocities obtained with HTLES3, upstream of the step, at $y/H = 0.557$ (corresponding to $y^+ \approx 84$). The results are normalized with the velocity, $U_h = 3U_H/2$, and the frequency step, Δ_ω. The cutoff frequency, $\omega_c = 50$ Hz, is higher than the maximum plotted frequency.

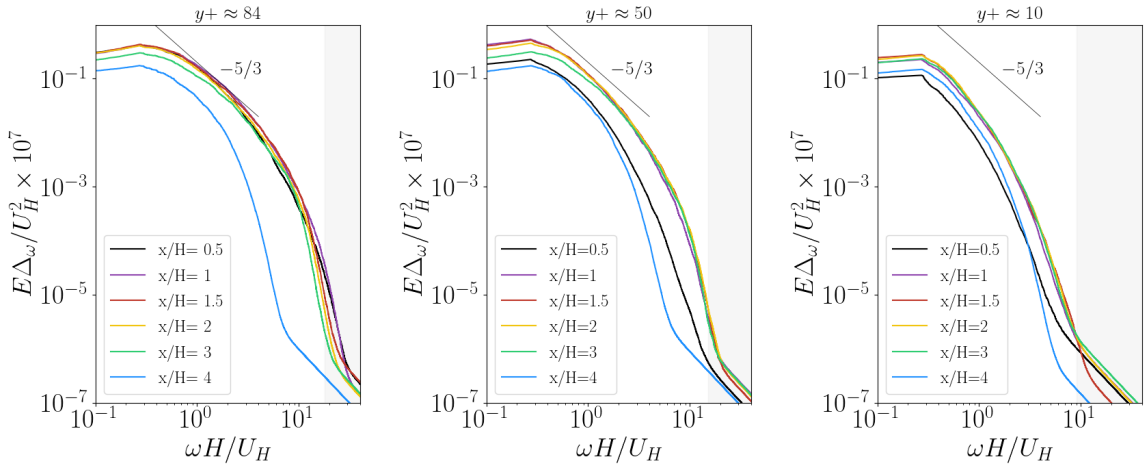

Fig. 16: Power spectral densities obtained with HTLES3 for $y/H = 1/3$, $y/H = 0.2$, and $y/H = 0.04$ (corresponding to $y^+ \approx 84$, $y^+ \approx 50$, and $y^+ \approx 10$, respectively), from left to right. The results are normalized with the velocity, U_H, and the frequency step, Δ_ω. The ranges in light gray color show frequencies higher than the cutoff frequency.

[9] B. Chaouat. "The State of the Art of Hybrid RANS/LES Modeling for the Simulation of Turbulent Flows". In: *Flow, Turbulence and Combustion* 99.2 (Sept. 2017), pp. 279–327. ISSN: 1573-1987.

[10] L. Chen, K. Asai, T. Nonomura, G. Xi, and T. Liu. "A Review of Backward-Facing Step (BFS) Flow Mechanisms, Heat Transfer and Control". In: *Thermal Science and Engineering Progress* 6 (June 2018), pp. 194–216. ISSN: 2451-9049.

[11] S. Deck. "Recent improvements in the Zonal Detached Eddy Simulation (ZDES) formulation". In: *Theor. Comput. Fluid Dyn.* 26.6 (2012), pp. 523–550.

[12] P. Druault, S. Lardeau, J.-P. Bonnet, F. Coiffet, J. Delville, E. Lamballais, J.-F. Largeau, and L. Perret. "Generation of Three-Dimensional Turbulent Inlet Conditions for Large-Eddy Simulation". In: *AIAA Journal* 42.3 (2004), pp. 447–456. ISSN: 0001-1452.

[13] V. Duffal, B. de Laage de Meux, and R. Manceau. "Development and Validation of a new formulation of Hybrid Temporal Large Eddy Simulation". In: *Flow Turbul. Combust.* 108 (2022), p. 42.

[14] V. Duffal, B. d. L. de Meux, and R. Manceau. "Development and Validation of a New Formulation of Hybrid Temporal Large Eddy Simulation". In: *Flow, Turbulence and Combustion* 108 (2022), p. 42.

[15] A. Fadai-Ghotbi, C. Friess, R. Manceau, and J. Borée. "A seamless hybrid RANS-LES model based on transport equations for the subgrid stresses and elliptic blending". In: *Phys. Fluids* 22.055104 (2010).

[16] A. Fadai-Ghotbi, C. Friess, R. Manceau, T. B. Gatski, and J. Borée. "Temporal Filtering: A Consistent Formalism for Seamless Hybrid RANS–LES Modeling in Inhomogeneous Turbulence". In: *International Journal of Heat and Fluid Flow*. Sixth International Symposium on Turbulence and Shear Flow Phenomena 31.3 (June 2010), pp. 378–389. ISSN: 0142-727X.

[17] J. Fröhlich and D. von Terzi. "Hybrid LES/RANS Methods for the Simulation of Turbulent Flows". In: *Progress in Aerospace Sciences* 44.5 (July 2008), pp. 349–377. ISSN: 0376-0421.

[18] R. García-Mayoral, D. Chung, P. Durbin, N. Hutchins, T. Knopp, B. J. McKeon, U. Piomelli, and R. D. Sandberg. "Challenges and Perspective on the Modelling of High-Re, Incompressible, Non-Equilibrium, Rough-Wall Boundary Layers". In: *Journal of Turbulence* 0.0 (), p. 2361738. ISSN: null.

[19] C. Geuzaine and J.-F. Remacle. "Gmsh: A 3-D Finite Element Mesh Generator with Built-in Pre- and Post-Processing Facilities". In: *International Journal for Numerical Methods in Engineering* 79.11 (2009), pp. 1309–1331. ISSN: 1097-0207.

[20] S. S. Girimaji. "Partially-Averaged Navier-Stokes Model for Turbulence: A Reynolds-Averaged Navier-Stokes to Direct Numerical Simulation Bridging Method". In: *Journal of Applied Mechanics* 73.3 (Nov. 2005), pp. 413–421. ISSN: 0021-8936.

[21] S. Heinz, R. Mokhtarpoor, and M. Stoellinger. "Theory-based Reynolds-averaged Navier-Stokes equations with large eddy simulation capability for separated turbulent flow simulations". In: *Physics of Fluids* 32.6 (2020).

[22] S. Heinz, R. Mokhtarpoor, and M. K. Stoellinger. "Hybrid RANS-LES Methods with Continuous Mode Variation". In: *Direct and Large Eddy Simulation XII*. Ed. by M. García-Villalba, H. Kuerten, and M. V. Salvetti. ERCOFTAC Series. Cham: Springer International Publishing, 2020, pp. 441–447. ISBN: 978-3-030-42822-8.

[23] G. Hyde-Linaker, P. Hall Barientos, S. Stoumpos, D. Kingsmore, and A. Kazakidi. "Patient-specific computational haemodynamics associated with the surgical creation of an arteriovenous fistula". In: *Med. Eng. Phys.* (2022), p. 103814. ISSN: 1350-4533.

[24] J. Janin, F. Duval, C. Friess, and P. Sagaut. "A New Linear Forcing Method for Isotropic Turbulence with Controlled Integral Length Scale". In: *Physics of Fluids* 33.4 (Apr. 2021), p. 045127. ISSN: 1070-6631.

[25] J. Jiménez. "Computing high-Reynolds-number turbulence: will simulations ever replace experiments?" In: *J. Turbul.* 4 (2003), pp. 1–14.

[26] A. Keating, G. De Prisco, and U. Piomelli. "Interface Conditions for Hybrid RANS/LES Calculations". In: *International Journal of Heat and Fluid Flow*. Special Issue of the 6th International Symposium on Engineering Turbulence Modelling and Measurements – ETMM6 27.5 (Oct. 2006), pp. 777–788. ISSN: 0142-727X.

[27] B. Krumbein, R. Maduta, S. Jakirlić, and C. Tropea. "A Scale-Resolving Elliptic-Relaxation-Based Eddy-Viscosity Model: Development and Validation". In: *New Results in Numerical and Experimental Fluid Mechanics XII*. Ed. by A. Dillmann, G. Heller, E. Krämer, C. Wagner, C. Tropea, and S. Jakirlić. Notes on Numerical Fluid Mechanics and Multidisciplinary Design. Cham: Springer International Publishing, 2020, pp. 90–100. ISBN: 978-3-030-25253-3.

[28] E. Lamballais. "Direct Numerical Simulation of a Turbulent Flow in a Rotating Channel with a Sudden Expansion". In: *Journal of Fluid Mechanics* 745 (Apr. 2014), pp. 92–131. ISSN: 0022-1120, 1469-7645.

[29] A. Limare, H. Borouchaki, and P. Brenner. "Adaptive Mesh Refinement with an Automatic Hybrid RANS/LES Strategy and Overset Grids". In: *Progress in Hybrid RANS-LES Modelling*. Ed. by Y. Hoarau, S.-H. Peng, D. Schwamborn, A. Revell, and C. Mockett. Notes on Numerical Fluid Mechanics and Multidisciplinary Design. Cham: Springer International Publishing, 2020, pp. 159–168. ISBN: 978-3-030-27607-2.

[30] R. Manceau. "Progress in Hybrid Temporal LES (invited keynote paper)". In: *Papers contributed to the 6th Symp. Hybrid RANS-LES Methods, 26–28 September 2016, Strasbourg, France*. Ed. by Y. Hoarau, S.-H. Peng, D. Schwamborn, and A. Revell. Vol. 137. Notes on Numerical Fluid Mechanics and Multidisciplinary Design. Springer, 2018, pp. 9–25.

[31] M. Mays, S. Lardeau, and S. Laizet. "Capturing the drag crisis in the flow around a smooth cylinder using a hybrid RANS-LES model on coarse meshes". In: *Int. J. Heat Fluid Fl.* 103 (2023), p. 109203.

[32] M. Mehta, R. Manceau, V. Duffal, and B. de Laage de Meux. "An active hybrid Reynolds-Averaged Navier-Stokes/large eddy simulation approach for gray area mitigation". In: *Phys. Fluids* 35.12 (2023), p. 125116.

[33] M. Mehta, R. Manceau, V. Duffal, and B. de Laage de Meux. "An Active Hybrid Reynolds-averaged Navier–Stokes/Large Eddy Simulation Approach for Gray Area Mitigation". In: *Physics of Fluids* 35.12 (Dec. 2023), p. 125116. ISSN: 1070-6631.

[34] F. R. Menter. "Two-Equation Eddy-Viscosity Turbulence Models for Engineering Applications". In: *AIAA Journal* 32.8 (Aug. 1994), pp. 1598–1605. ISSN: 0001-1452.

[35] F. R. Menter and Y. Egorov. "The Scale-Adaptive Simulation Method for Unsteady Turbulent Flow Predictions. Part 1: Theory and Model Description". In: *Flow, Turbulence and Combustion* 85.1 (July 2010), pp. 113–138. ISSN: 1573-1987.

[36] F. Menter and Y. Egorov. "The Scale-Adaptive Simulation Method for Unsteady Turbulent Flow Predictions. Part 1: Theory and Model Description". In: *Flow Turbulence and Combustion* 85 (July 2010), pp. 113–138.

[37] M. A. Park, A. Loseille, J. Krakos, T. R. Michal, and J. J. Alonso. "Unstructured Grid Adaptation: Status, Potential Impacts, and Recommended Investments Towards CFD 2030". In: *46th AIAA Fluid*

Dynamics Conference. Washington, D.C.: American Institute of Aeronautics and Astronautics, June 2016. ISBN: 978-1-62410-436-7.

[38] J. B. Perot and J. Gadebusch. "A Self-Adapting Turbulence Model for Flow Simulation at Any Mesh Resolution". In: *Physics of Fluids* 19.11 (Nov. 2007), p. 115105. ISSN: 1070-6631.

[39] J. B. Perot and J. Gadebusch. "A Stress Transport Equation Model for Simulating Turbulence at Any Mesh Resolution". In: *Theoretical and Computational Fluid Dynamics* 23.4 (July 2009), pp. 271–286. ISSN: 1432-2250.

[40] S. B. Pope. "Ten Questions Concerning the Large-Eddy Simulation of Turbulent Flows". In: *New Journal of Physics* 6.1 (Mar. 2004), p. 35. ISSN: 1367-2630.

[41] S. Reuß, T. Knopp, A. Probst, and M. Orlt. "Assessment of Local LES-Resolution Sensors for Hybrid RANS/LES Simulations". In: *Progress in Hybrid RANS-LES Modelling*. Ed. by S. Girimaji, W. Haase, S.-H. Peng, and D. Schwamborn. Notes on Numerical Fluid Mechanics and Multidisciplinary Design. Cham: Springer International Publishing, 2015, pp. 93–103. ISBN: 978-3-319-15141-0.

[42] M. L. Shur, P. R. Spalart, M. K. Strelets, and A. K. Travin. "A Hybrid RANS-LES Approach with Delayed-DES and Wall-Modelled LES Capabilities". In: *International Journal of Heat and Fluid Flow* 29.6 (Dec. 2008), pp. 1638–1649. ISSN: 0142-727X.

[43] P. R Spalart. "Strategies for Turbulence Modelling and Simulations". In: *International Journal of Heat and Fluid Flow* 21.3 (June 2000), pp. 252–263. ISSN: 0142-727X.

[44] P. R. Spalart and V. Venkatakrishnan. "On the Role and Challenges of CFD in the Aerospace Industry". In: *The Aeronautical Journal* 120.1223 (Jan. 2016), pp. 209–232. ISSN: 0001-9240, 2059-6464.

[45] H. Tennekes. "Eulerian and Lagrangian Time Microscales in Isotropic Turbulence". In: *Journal of Fluid Mechanics* 67.3 (Feb. 1975), pp. 561–567. ISSN: 1469-7645, 0022-1120.

[46] T. Tran, R. Manceau, R. Perrin, J. Borée, and A. Nguyen. "A hybrid temporal LES approach. Application to flows around rectangular cylinders". In: *Proc. 9th ERCOFTAC Int. Symp. on Eng. Turb. Modelling and Measurements, Thessaloniki, Greece*. 2012.

[47] S. Woodruff. "Adaptive Embedded LES of the NASA Hump". In: *AIAA Scitech 2019 Forum*. eprint: https://arc.aiaa.org/doi/pdf/10.2514/6.2019-1649.